# The role of dilation and confining stresses in shear thickening of dense suspensions

Eric Brown and Heinrich M. Jaeger
James Franck Institute, The University of Chicago, Chicago, IL 60637

March 21, 2011

**Abstract**

Many densely packed suspensions and colloids exhibit a behavior known as Discontinuous Shear Thickening in which the viscosity jumps dramatically and reversibly as the shear rate is increased. We performed rheometry and video microscopy measurements on a variety of suspensions to determine the mechanism for this behavior. We distinguish Discontinuous Shear Thickening from inertial effects by showing that the latter are characterized by a Reynolds number but are only found for lower packing fractions and higher shear rates than the former. If the suspended particles are heavy enough to settle we find the onset stress of shear thickening $\tau_{min}$ corresponds to a hydrostatic pressure from the weight of the particle packing. Combined with previous results for colloids this suggests that generally $\tau_{min}$ corresponds to the stress required to shear neighboring particles relative to each other. Shear profiles and normal stress measurements indicate that, in the shear thickening regime, stresses are transmitted through frictional rather than viscous interactions. Above $\tau_{min}$, dilation is seen to cause particles to penetrate the liquid-air interface of the sheared sample. The upper stress boundary $\tau_{max}$ of the shear thickening regime is shown to roughly match the ratio of surface tension divided by a radius of curvature on the order of the particle size. These results suggest a new model in which the viscosity jump comes from frictional stresses due to a confining stress from surface tension as the liquid-air interface at the boundary is deformed by dilation. A similar change in boundary conditions happens without shear when the packing fraction is increased above the jamming transition, where a yield stress on the scale of $\tau_{max}$ develops as a result of particles penetrating the liquid-air interface. We generalize this shear thickening mechanism to other sources of a confining stress by showing that, when instead the suspensions are confined by solid walls and have no liquid-air interface, $\tau_{max}$ is set by the stiffness of the most compliant boundary. With these new scaling laws, we can delineate the shear thickening regime in a phase diagram that encompasses the scalings found not only for suspensions but also colloids with Brownian and electrostatic interactions. All of this rheology can be described by a non-local constitutive relation which is locally shear thinning, but where the viscosity jump comes from a normal stress term which depends on the global dilation.

## 1 Introduction

Shear thickening is a category of non-Newtonian fluid behavior in which the viscosity $\eta = \tau/\dot{\gamma}$ increases as a function of shear rate $\dot{\gamma}$ or shear stress $\tau$ over some parameter range. A particularly dramatic form, often called Discontinuous Shear Thickening (Metzner and Whitlock, 1958; Hoffman, 1972; Barnes, 1989; Maranzano and Wagner, 2001a), occurs in many densely packed suspensions and colloids such as cornstarch in water. These suspensions feel like a thin liquid at low stresses, but become very thick and can even crack like a solid at higher stresses, and become thin again when the stress is removed. Such materials are of practical interest for their properties as dampeners and shock absorbers (Lee et al., 2003; Shenoy et al., 2003; Jolly and Bender, 2006). While there are various models to describe shear thickening, and some milder types of shear thickening are attributed to viscous Brady and Bossis (1985) or inertial (Bagnold, 1954) effects, prior approaches have not been very successful at describing the dramatic effects found in dense suspensions. Our goal with this paper is to propose and test a general mechanism for Discontinuous Shear Thickening. This problem can be broken down into several main questions: under what conditions will a suspension or colloid exhibit Discontinuous Shear Thickening?, what are the scaling laws that determine the parameter range of shear thickening?, what is the form of the constitutive law?, and can it occur in systems other than suspensions and colloids? We will use a wide variety of rheometry and video microscopy measurements to fully answer the above

questions. Our approach differs from previous work in that we consider a granular point of view in addition to the traditional hydrodynamic approach.

The remainder of this paper is organized as follows. In Sec. 2 we review the literature on shear thickening to characterize what is generally known about Discontinuous Shear Thickening. In Sec. 3 we describe the rheometry techniques and suspensions used in our experiments. In Sec. 4 we show viscosity curves for shear thickening suspensions at different packing fractions and liquid viscosities. With this we can test inertial hydrodynamic scalings which we find to be relevant in a different parameter regime than Discontinuous Shear Thickening. In Sec. 5 we show measurements of the onset stress $\tau_{min}$ of shear thickening for different particle sizes and liquid densities to quantify the effect of gravity on $\tau_{min}$. In Sec. 6 we show shear profile measurements with different liquid densities to ascertain the role of gravity in the shape of the shear profile and how it changes in different rheological regimes. We use these shear profiles to test a proposed constitutive law, and come to the surprising conclusion that the shear stress is not directly dependent on the local shear rate in the shear thickening regime. In Sec. 7 we show shear and normal stress measurements with different boundary conditions. From this we find a global constitutive relation that is frictional rather than viscous, which suggests mechanics similar to soils or granular flows. In Sec. 8 we use images of the surface of the suspensions at rest for different packing fractions to show that the onset of a yield stress coincides with a visible change at the suspension-air boundary as particles penetrate the liquid-air interface. We also show that a similar visible change occurs along with shear thickening due to dilation of the granular packing under shear. In Sec. 9 we propose that this boundary condition results in a confining stress due to surface tension at the liquid-air interface which can set the scale of the stress response to shear. We then show that comparisons of the measured stress and dilation are consistent with this model, and that the confining stress scale from surface tension agrees with measurements of the maximum stress in the shear thickening regime $\tau_{max}$ for different suspensions over a wide range of particle sizes. In Sec. 10 we generalize this result to other sources of confining stress with measurements from a rheometer with solid walls instead of a liquid-air interface at the boundary and show that $\tau_{max}$ is generally set by the stiffness of the boundary. In Sec. 11 we combine our measurements of $\tau_{min}$ and $\tau_{max}$ with other scalings found in different parameter regimes to delineate typical boundaries of the shear thickening regime for suspensions and colloids, and write a general constitutive relation for these systems. Finally, we summarize the general conditions for Discontinuous Shear Thickening.

# 2 Background

Because of the vast amounts of literature referring to different phenomena and mechanisms which all fall under the category of shear thickening, we first carefully define what we call Discontinuous Shear Thickening, then review the literature that applies to Discontinuous Shear Thickening. We will suggest based on the literature that hydrodynamic models which have been successful for describing other types of shear thickening have been insufficient for describing Discontinuous Shear Thickening. Rather, there is significant evidence supporting the importance of dilation and normal forces which suggests we should additionally consider a granular point of view.

Discontinuous Shear Thickening (Metzner and Whitlock, 1958; Hoffman, 1972, 1974, 1982; Barnes, 1989; Boersma et al., 1990; Laun, 1994; Frith et al., 1996; Bender and Wagner, 1996; O'Brien and Mackay, 2000; Maranzano and Wagner, 2001a,b, 2002; Bertrand et al., 2002; Lootens et al., 2003, 2005; Egres and Wagner, 2005; Shenoy and Wagner, 2005; Egres et al., 2006; Lee and Wagner, 2006; Fall et al., 2008; Brown and Jaeger, 2009; Brown et al., 2010a,b) can be characterized by a few properties, which are observed to be similar in both dense suspensions and colloids. Thus we find it convenient to define the phenomenon of Discontinuous Shear Thickening based on these properties and to distinguish it from other types of shear thickening:

1. Stress scales: The boundaries of the shear thickening regime are simply described in terms of stress scales (rather than shear rate) which are mostly independent of packing fraction (Maranzano and Wagner, 2001a; Shenoy and Wagner, 2005; Brown and Jaeger, 2009) and liquid viscosity (Boersma et al., 1990; Frith et al., 1996). Consequently, the onset shear rate varies with packing fraction and liquid viscosity since suspension viscosities increase with both parameters (Brady and Bossis, 1985). Shear thinning or Newtonian behavior is found at lower stresses below the onset of shear thickening at a stress $\tau_{min}$. Above the upper stress boundary of the shear thickening regime $\tau_{max}$, shear thinning is usually found.
2. Diverging slope: The term 'Discontinuous' refers to the apparent discontinuous jump in $\tau(\dot{\gamma})$ of orders of magnitude at the onset of shear thickening. This jump is only observed at very high particle packing fractions (around 0.5 for nearly spherical particles). The slope of $\tau(\dot{\gamma})$ is only very steep over a small range in packing fraction (a few percent), lessening significantly at lower packing fractions (Maranzano and Wagner, 2001a; Egres and Wagner, 2005; Brown and Jaeger, 2009). The packing fraction dependence of the slope of $\tau(\dot{\gamma})$ can be characterized as a power law diverging at a packing fraction $\phi_c$ (Brown and Jaeger, 2009). Above $\phi_c$ the system is jammed meaning it will not flow for applied stresses below a non-zero yield stress of scale $\tau_j$.

3. Reversibility: The Discontinuous Shear Thickening described above is reversible, meaning viscosity curves are similar whether they are measured with increasing or decreasing stress histories. Some examples of dramatic shear thickening have been found to be irreversible because of chemical-attraction-induced aggregation (Osuji et al., 2008; Larsen et al., 2010) or occur only in transient behavior (Fall et al., 2010), and will not be considered here as they may be different phenomena.

Because the above features of Discontinuous Shear Thickening are similar in both the suspension and colloid regimes, we refer to data in both regimes. While the dominant forces tend to be different, we will ultimately describe a generic mechanism that can apply to both regimes but results in different scaling laws depending on the dominant forces.

To facilitate an understanding of Discontinuous Shear Thickening, it may useful up front to appreciate a disconnect between local and global viewpoints of rheology. Standard rheology experiments measure a global mechanical response based on the drag force required to move two solid surfaces at some speed relative to each other with a fluid in between. This is in contrast to the hydrodynamic theory of rheology which is based on continuum equations consisting of local constitutive relations between shear stress and shear rate. One of the surprising results presented in this paper is that the global and local viewpoints of rheology lead to drastically different conclusions in the shear thickening regime of the dense suspensions being investigated. Historically, Discontinuous Shear Thickening has been defined in previous experiments based on measurements of the global mechanical response. We will show in Sections 6 that the constitutive relation based only on the local shear rate can actually be *shear thinning* instead of shear thickening for these suspensions. To resolve this apparent contradiction, in Sec. 7 we will show that most of the shear stress is due to frictional interactions which depend on the normal stress rather than the local shear rate. Because the two standard viewpoints disagree on whether these dense suspensions are shear thickening or shear thinning, there will be some difficulty with terminology. We chose to continue using the terminology of Discontinuous Shear Thickening to keep the connection to the previous literature, where the term is used extensively. As a compromise with the local viewpoint, we have chosen to capitalize 'Discontinuous Shear Thickening' to refer to it as a name for a phenomenon rather than a description, since from the local viewpoint it would not qualify as shear thickening. The goal of this paper is to understand the global phenomenon of Discontinuous Shear Thickening, regardless of the local constitutive relations.

In contrast to the Discontinuous Shear Thickening described above, there are other types of shear thickening with different characteristics that can be described in hydrodynamic terms. One type is described by a Peclet number which is the ratio of advective to diffusive transport of particles (Bergenholtz et al., 2002). The shear thickening found in these models is relatively very weak in the sense that the viscosity increases by only a few percent per decade of shear rate (Brady and Bossis, 1985; Melrose and Ball, 2001a). Inertial effects can also result in shear thickening, described in terms of either a Reynolds number or Bagnold number, in which inertial stresses can be characterized by $\tau(\dot{\gamma}) \propto \dot{\gamma}^2$ in the limit of high shear rate (Bagnold, 1954). In each of these cases, the onset of shear thickening is characterized by a shear rate, in contrast to an onset stress for Discontinuous Shear Thickening. Because of the less steep $\tau(\dot{\gamma})$, such shear thickening is often called Continuous Shear Thickening. If the stress/shear-rate relation in the shear thickening regime is expressed as $\tau \sim \dot{\gamma}^{1/\varepsilon}$, we can thus identify shear thickening as Discontinuous if $1/\varepsilon > 2$ can be observed at high packing fractions and $1/\varepsilon$ increases with packing fraction, and Continuous if $1/\varepsilon \leq 2$ at all packing fractions. Continuous Shear Thickening can be observed even at very low packing fractions and has a much weaker packing fraction dependence than Discontinuous Shear Thickening. In Sec. 4 we will show an example of inertial shear thickening and characterize the parameter regime where it occurs in so we can clearly separate Discontinuous Shear Thickening from inertial stresses.

Because of the qualitative differences between Discontinuous and Continuous Shear Thickening, we suspect they are different phenomena with different mechanisms, and focus here only on Discontinuous Shear Thickening [1]. For this reason, we will not assume that results that apply to Continuous Shear Thickening also apply to Discontinuous Shear Thickening. This is a different approach from much of the literature which has tended to apply a single hydrodynamic model to both Continuous and Discontinuous Shear Thickening (Brady and Bossis, 1985; O'Brien and Mackay, 2000; Maranzano and Wagner, 2001a; Gopalikrishnan and Zukoski, 2004; Osuji et al., 2008; Wagner and Brady, 2009). The idea with the earlier approach has been to start with the hydrodynamic models of Continuous Shear Thickening which are well-understood at low packing fractions (Bergenholtz et al., 2002), and extend them to higher packing fractions. The expectation is that at higher packing fractions, hydrodynamically-induced clusters of particles form in which nearby particles act transiently as a solid cluster when they get so close to each other that the lubrication drag force between them blows up (Brady and Bossis, 1985; Farr et al., 1997). While this mechanism seems plausible, so far the calculations have failed to reproduce steep viscosity curves comparable to experimental

[1] In some of the literature a distinction is made between discontinuous and continuous shear thickening at different packing fractions based solely on the slope of the viscosity curve. However, in many cases there is no qualitative change in behavior or identifiable transition in scaling when the packing fraction is varied. Thus we do not follow this convention because it does not suggest different phenomena.

measurements of Discontinuous Shear Thickening.

The major success of these models for Discontinuous Shear Thickening is the calculation of the stress at the onset of shear thickening $\tau_{min}$. In early models for Brownian-motion dominated colloids the onset was described by a critical Peclet number $Pe = 6\pi\eta\dot{\gamma}a^3/kT$ for a particle size $a$ and thermal energy $kT$. Shear thickening is expected to occur for $Pe \gg 1$ as the shear stress overcomes thermal diffusion of the particles (Brady and Bossis, 1985; Melrose and Ball, 2001a). However, observations found the onset of shear thickening to be determined by the same stress at different packing fractions rather than the same shear rate. This model, when using the suspension viscosity to convert to a stress scale $\tau = \eta\dot{\gamma} = kT/6\pi a^3$, has been successful at calculating the onset of both Continuous and Discontinuous Shear Thickening (Gopalikrishnan and Zukoski, 2004; Maranzano and Wagner, 2001b). For colloids where repulsions from a zeta potential $\zeta$ are dominant the above model had to be modified (Maranzano and Wagner, 2001a). In that case, the particular scaling found was a stress $\tau \sim \epsilon\zeta^2/a^2$ for permittivity $\epsilon$ characterizing electrostatic particle interactions.[2] In each case, the modifications to the hydrodynamic model required to fit it to the data resulted in completely eliminating any dependence on hydrodynamic parameters such as viscosity or shear rate. Therefore, the resulting onset stress scale is not specific to hydrodynamic mechanisms, as any type of force transferred through a continuum system can be expressed in terms of a stress. Not surprisingly, with several relevant forces in colloids and suspensions, each of which could be dominant in different cases, a variety of different scalings for the onset stress have been found. Depending on the parameter range, this dominant force could be Brownian motion (Bergenholtz et al., 2002; Gopalikrishnan and Zukoski, 2004), zeta potential (Maranzano and Wagner, 2001a), induced dipole attractions (Brown et al., 2010a), or steric repulsion (Hoffman, 1998). Notably, in each case hydrodynamic terms such as shear rate and viscosity were found to be absent from the modified scalings required to match the experiments. This suggests inertia or hydrodynamics-based models are not necessary to determine the onset of Discontinuous Shear Thickening as initially envisioned by the Peclet number scalings. We will revisit the subject of the onset stress in Sec. 5.

Another observation that the hydrodynamic models require modification to describe is the upper stress boundary of the shear thickening regime $\tau_{max}$, since for inertial effects the viscosity increases monotonically with shear rate. It has been suggested that this could be fixed by accounting for the finite stiffness of particles (Wagner and Brady, 2009), but again this is not necessarily a hydrodynamic correction. We will address the issue of the upper stress boundary in Sec. 9.

We could simply approach the problem in terms of stress scales as a modification of hydrodynamic models as many others have done (Maranzano and Wagner, 2001a; O'Brien and Mackay, 2000; Gopalikrishnan and Zukoski, 2004; Osuji et al., 2008). Instead, here we focus on the scaling laws for the stress scales $\tau_{min}$ and $\tau_{max}$ to gain insight into the relevant physical mechanisms and come up with a description that encompasses all of these scalings without the need to refer to a hydrodynamic model. A major advantage of this approach is that different mechanisms such as interparticle forces, gravity, and surface tension can be simply expressed in terms of stress scales which can be compared to the measured stresses without the need to reference a base model. Another good reason to try to understand Discontinuous Shear Thickening without reference to hydrodynamic models is that some features of the rheology that suggest a granular rather than hydrodynamic perspective on the system.

Granular materials can have properties of solids, liquids, or gases under different conditions (Jaeger et al., 1996). For example, randomly packed particles at high enough packing fractions cannot shear or compress because geometric constraints force them to be in contact, so they have a yield stress like a solid. At lower packing fraction the particles are able to move around each other freely in a liquid-like state. The transition between these two regimes is sharp and is known as the jamming transition (Liu and Nagel, 1998; O'Hern et al., 2003). For shear thickening suspensions, the divergence of the slope of $\tau(\dot{\gamma})$ at a critical packing fraction $\phi_c$ was found to correspond to the jamming transition (Brown and Jaeger, 2009).

Forces tend to be transmitted through jammed granular packings along concentrated paths called force chains (Cates et al., 1998) such that the distribution of forces is characterized by an exponential tail (Mueth et al., 1998; Majmudar and Behringer, 2005; Corwin et al., 2005). Simulations of shear thickening colloids have similarly found contact networks between particles with an exponential distribution of forces under shear (Melrose and Ball, 2004b).

A feature of granular shear flows with special relevance to shear thickening is dilation (Reynolds, 1885; Onoda and Liniger, 1990). When a granular packing is sheared, the particles have to go around each other so the packing dilates, taking up more volume than it does at rest. It has long been known that dilation occurs along with Discontinuos Shear Thickening (see Metzner and Whitlock (1958), and references therein). In fact, in some of the literature 'dilatancy' has been used as a synonym for shear thickening (Barnes, 1989). Especially important in understanding this relationship was the paper by Metzner and Whitlock. They showed that for suspensions of 0.2-1 $\mu$m $TiO_2$ particles, dilation initiated at stresses close to the onset of shear thickening for a range of packing fractions. However,

[2]While the forces were calculated at a distance corresponding to an effective hydrodynamic radius, calculating at a different radius would only change a scale factor of order 1, and since the model was an order-of-magnitude calculation, it would have resulted in just as good a match with the data.

they found suspensions of 28-100 $\mu$m glass spheres in sucrose solutions dilated but did not shear thicken, showing that dilation was not always equivalent to shear thickening. For 40+ years following this result, many of the major papers on shear thickening dropped the focus on dilation in favor of hydrodynamic descriptions (Hoffman, 1982; Brady and Bossis, 1985; Maranzano and Wagner, 2001a).

However, there is another possible interpretation of the data presented by Metzner and Whitlock (1958). They confirmed for several suspensions that the onset of shear thickening coincided with dilation, as had been seen in many previous results (see references in Metzner and Whitlock (1958)). Taken together with the observation of dilation in the absence of shear thickening, this inductively suggests that dilation is necessary but not sufficient for Discontinuous Shear Thickening. More recent results have shown that shear thickening can be hidden by a yield stress or other shear thinning effect (Brown et al., 2010a). In particular, Metzner and Whitlock used glass beads ranging from 28-100 $\mu$m in diameter in a Couette geometry, and such large, heavy particles will jam in a Couette cell because they settle under gravity, resulting in a yield stress (Fall et al., 2009). This can explain why shear thickening was not observed for the settling particles used by Metzner and Whitlock. It has only been in the last 10 years that dilation has become prominent again in the shear thickening literature (O'Brien and Mackay, 2000; Lootens et al., 2003, 2005; Fall et al., 2008). However, a mechanism by which dilation leads to a dramatic increase in stress has yet to be explained. This is the subject of Sections 8, 9, and 10.

When dilation of granular shear flows is prevented by confinement, shear is instead accompanied by normal forces against the walls (Reynolds, 1885; Onoda and Liniger, 1990). For Discontinuous Shear Thickening suspensions normal forces are usually found to be positive, meaning the sample is pushing against the rheometer plate as expected for dilation (Jomha and Reynolds, 1993; Lootens et al., 2003, 2005; Fall et al., 2008; Brown et al., 2010b). It was proposed by Fall et al. (2008) that shear thickening cannot occur if the normal stress is taken away. We will test this in Sec. 7.

# 3 Materials and methods

## 3.1 Tools

Measurements were performed with an Anton Paar Physica MCR 301 rheometer which measures the torque $T$ required to shear a sample at a tool angular rotation rate $\omega$. Most measurements were done in a parallel plate setup where normal forces could be measured. This geometry is shown in Fig. 1a and characterized by the plate radius $R = 12.5$ or 25 mm and gap size $d$ between the plates. A few measurements were done with a cylindrical cup-and-bob (Couette) geometry in which the environment is better controlled. The tool surfaces are smooth stainless steel. The viscosity, indicating the mechanical resistance to shear, is defined as $\eta \equiv \tau/\dot{\gamma}$ in a steady state. For the parallel plate setup, for example, we represent the global shear stress by

$$\tau = \frac{2T}{\pi R^3} \tag{1}$$

and shear rate by

$$\dot{\gamma} = \frac{R\omega}{d} \ . \tag{2}$$

These standard coefficients give the local stress at the edge of the plate in the case of a Newtonian shear profile, but may overestimate it by as much as 25% for different shear profiles. The reported global shear stress and shear rate values are meant to characterize the mechanical response in a way that is independent of system size so it can be compared to other physically relevant stress scales.

In the parallel plate measurements, the upward force on the rheometer tool is measured and the mean normal stress $\tau_N$ is obtained by dividing this normal force by the plate cross-sectional area. The standard deviation of the force measured during a static measurement over 10 s intervals with or without sample is $6 \times 10^{-4}$ N, giving a relative uncertainty of 0.3 Pa (1.2 Pa) for a 50 mm (25 mm) diameter plate. The standard deviation of the average force measured after calibration with no sample is $4 \times 10^{-3}$ N, giving an absolute uncertainty of 2 Pa (8 Pa) for a 50 mm (25 mm) diameter plate. The resolution of the shear stress is much better, with an absolute uncertainty less than (0.001 Pa) 0.01 Pa for a 50 mm (25 mm) plate.

The Anton Paar MCR 301 rheometer has special settings for normal force control measurements. Our reported measurements were done with the value of 'normal force hysteresis' set to 0.001 N. This value controls how much the normal force can deviate from the set value before the plate moves in response, although in practice the plate tends not to move until the normal force deviation exceeds about 0.01 N (20 Pa for the 25 mm plate). The 'normal force dynamics' value was set to 0% (default). This value controls the acceleration of the gap size in the feedback loop. This setting corresponds to the most reproducible steady state gap sizes, and the slowest acceleration of the gap, so it responds slowly to variations in the normal force.

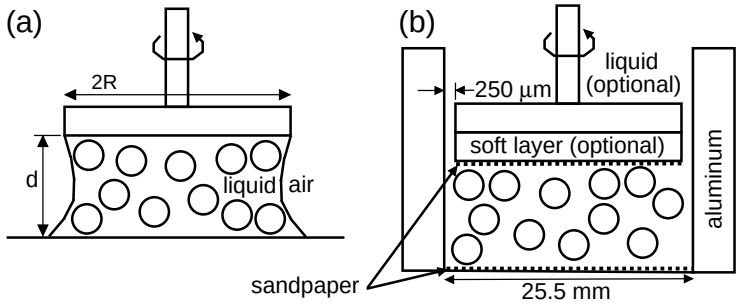


Figure 1: (a) A standard parallel plate rheometer setup. The suspension is confined between the plates by the surface tension of the suspending liquid. (b) A modified parallel plate setup with solid walls around the sample. In this setup the use of a suspending liquid is optional, and the wall stiffness can be modified by inserting layers of different stiffness between the suspension and plate.

The typical parallel plate setup is shown in Fig. 1a, in which the suspension is held in place between the parallel plates by surface tension at the liquid-air interface around the side. Because we saw that particles could penetrate the liquid-air interface (see Sec. 8) which we suspected could modify the stresses on the suspension from the interfacial tension, we desired a different boundary condition with a hard wall for some experiments. To accomplish this we machined an aluminum cylindrical cup with inner diameter 25.5 mm as shown in Fig. 1b. The cup fits around the tool with a gap small enough to prevent 500 $\mu$m diameter particles from slipping through but large enough to allow the tool to rotate without friction. This cup confined the particles to the volume beneath the plate, while the liquid could be filled to a higher level or omitted altogether so there was no liquid-air interface for particles to penetrate. The plates were covered with sandpaper sheets with a grit size of 100 $\mu$m to avoid slip with dry grains. In some cases we inserted a soft layer in between the top plate and the sandpaper to modify the compliance of the wall.

## 3.2 Suspensions

We studied suspensions with a variety of particle types and liquids to propose and test a model that explains a mechanism for Discontinuous Shear Thickening. The intent is that this model be universal, meaning that it applies equally to all suspensions and is not limited to a specific suspension. Thus, to develop and test such a general model, we investigated several suspensions, all of which the model must describe, and focus on reporting the features that are common to all suspensions we could test.

As a prototypical shear thickener we used cornstarch obtained from Argo. Cornstarch particles have a mean diameter of 14 $\mu$m and density of 1.59 g/mL based on buoyancy in CsCl solutions. They are very hydrophilic and hard – with a compression modulus on the order of $10^{10}$ Pa – at room temperature. At higher temperatures the polymers that compose cornstarch particles can gel. To compare suspensions with different liquid viscosities, we suspended cornstarch in either a mixture of 61.5% water and 38.5% CsCl by weight with a viscosity of 1 mPa·s and density of 1.41 g/mL or a mixture of 73.5% glycerol 13.0% water, and 13.5% CsCl by weight with a viscosity of 80 mPa·s and density of 1.34 g/mL. For such small particles, the settling time is several hours even without density matching.

For a series of suspensions in which we varied particle size we used soda-lime glass spheres with a density of 2.46 g/mL. We obtained particles with nominal diameter ranges of 3-10 $\mu$m, 10-25 $\mu$m, and 15-40 $\mu$m from Corpuscular, 45-63 $\mu$m, 75-104 $\mu$m (referred to as 100 $\mu$m), 177-250 $\mu$m, and 400-595 $\mu$m from MoSci (Class IV), and 1120-1350 $\mu$m and 1900-2100 $\mu$m. For polydisperse suspensions, no observable effect on the onset stress $\tau_{min}$ has been found since data can be collapsed based on the geometric mean particle size (Maranzano and Wagner, 2001a), thus we will compare particle distributions only by their mean diameter. The glass spheres were dispersed in various liquids, including water or mineral oil with a viscosity of 58 mPa·s and density of 0.87 g/mL.

For visualization purposes we used two types of opaque particles. The first, referred to as $ZrO_2$, were spheres obtained from Glen Mills consisting of 69% $ZrO_2$ and 31% $SiO_2$. They have a nominal diameter range of 100-200 $\mu$m and a density of 3.8g/mL. These particles were dispersed in the same mineral oil used for the glass particles. For experiments with density matched suspensions, we used polyethylene spheres obtained from Cospheric. These particles have a nominal diameter range of 125-150 $\mu$m and density of 1.01 g/mL. They were dispersed in silicone oil AR 20 with a nominal density of 1.01 g/mL and viscosity of 20 mPa·s. When varying the temperature of the suspension, we found that the settling time was minimized at 19° C from which we estimated a density difference of order $10^{-4}$ g/mL.

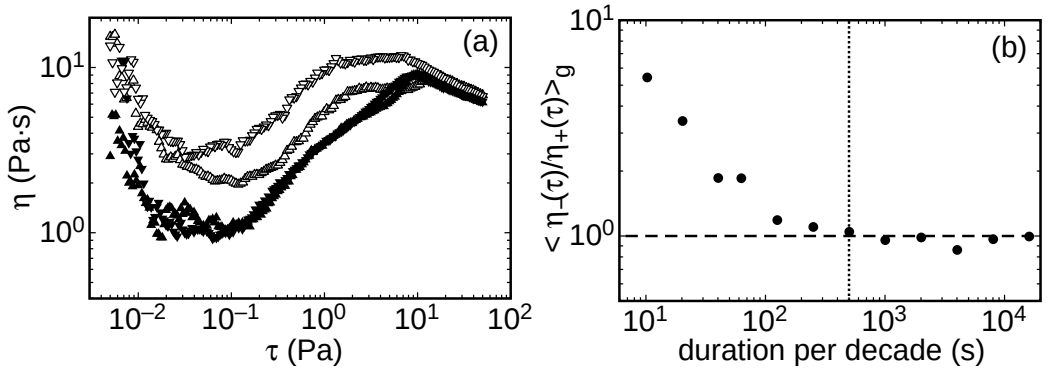


Figure 2: (a)Apparent viscosity curves for 100 $\mu$m glass spheres in mineral oil taken with different measurement durations to show hysteresis loops. Open symbols: measurement duration of 40 s per decade of the stress ramp. Solid symbols: 500 s per decade. Up-pointing triangles correspond to increasing stress ramps, while down-pointing triangles correspond to decreasing stress ramps. (b) Characterization of the hysteresis as the geometric mean of the viscosity ratio between the decreasing and increasing ramps of the hysteresis loop, plotted for different ramp durations per decade of stress. Dashed line: a ratio of 1 between increasing and decreasing ramps corresponding to no hysteresis. Dotted line: ramp rate used for later steady state measurements

We also include some summary data for particles fabricated into different shapes from polyethylene glycol (PEG) (see Brown et al. (2010a) for details) suspended in liquid PEG-250, and 100 $\mu$m spheres made of polystyrene dimethyl ether suspended in PEG.

### 3.3 Measurement procedure

Measurements were made with the rheometer's bottom plate temperature controlled at 20° C. The room humidity ranged from 22% to 38%, although during individual experiments the humidity was constant. This affects the amount of evaporation/adsorption of water from/to suspensions which can result in an apparent time dependence in measurements due to the sensitive packing fraction dependence of shear thickening suspensions (Brown and Jaeger, 2009). To minimize evaporation or adsorption, we used a solvent trap when the suspending liquid was water which enclosed the sample and a small amount of air around it by an extra layer of liquid. The enclosed air equilibrated with the sample to prevent further changes to the suspension.

Packing fractions $\phi$ were measured as the volume of solid particles over the total volume of solids plus liquid. The packing fraction in terms of the inverse of the available free volume per particle may decrease slightly during measurements as the grain packing dilates. Above the jamming transition, the packing fraction may also be less than the measured packing fraction if air bubbles become trapped in the interior. Humidity also has a large effect on the amount of water adsorbed onto dry grains open to the atmosphere, especially cornstarch which is so hygroscopic that 10-20% of the weight of the 'dry' powder is from water. Comparison of density measurement techniques suggest that cornstarch is porous or that it may absorb CsCl, thus we report mass fractions $\phi_m$ for cornstarch rather than volumetric packing fractions. For the humidity conditions and CsCl concentrations used, the jamming transition occurs at about the same mass fraction in cornstarch suspensions as the packing fraction for frictional spheres ($\phi_c = 0.56$ for cornstarch in water, $\phi_c = 0.58$ for cornstarch in the glycerol-water mixture, and $\phi_c = 0.57$ for frictional spheres). Thus the mass fractions for cornstarch suspensions roughly correspond to packing fractions for sphere suspensions under our experimental conditions, but we note this is just a coincidence and comparing packing fractions of cornstarch suspensions under different conditions is not trivial.

The gap size $d$ for parallel plate measurements was usually about 1 mm, large enough to avoid finite-size effects on the viscosity for particles around 100 $\mu$m in diameter (Brown et al., 2010b). We measured bulk shear thickening with both rough and smooth plates and did not find any difference in the shear thickening due to the plate surface. To directly measure slip, we used video microscopy to observe the shear profile at the outer edge of the plate. The results of these measurements are shown in Sec. 6. We visually confirmed that the suspensions do not spill for all reported measurements. Spillage was often the limiting factor in the maximum stress or shear rate applied for our measurements.

Viscosity curves were measured by first pre-shearing immediately before measurements for at least 100 seconds at shear rates above the shear thickening regime where the steady state flow is fully mobilized, then ramping the

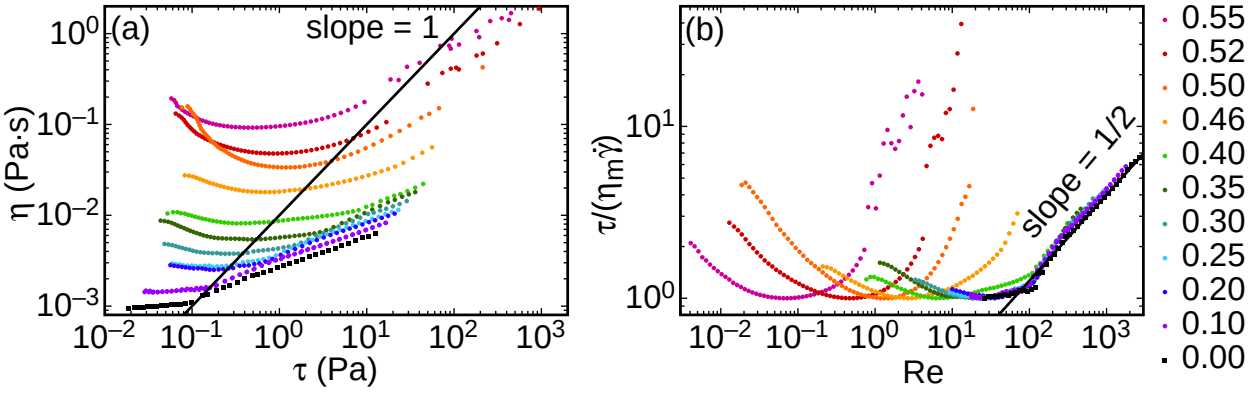


Figure 3: (a) Viscosity vs. stress curves for suspensions of cornstarch in water. Mass fractions $\phi_m$ are shown in the key; higher curves correspond to larger $\phi_m$. The solid line corresponds to a constant shear rate. (b) A rescaling of the data as $\tau/\eta_m\dot{\gamma}$ vs. Reynolds number $Re = \rho_l\dot{\gamma}d^2/\eta_m$ which should result in a data collapse for hydrodynamic flows. The line corresponds to a scaling $\tau \sim \dot{\gamma}^{3/2}$ in the range $100 \lesssim Re \lesssim 3000$.

control parameter (shear stress or rate) down and then up to obtain hysteresis loops. To ensure that we obtain steady state viscosity curves, the measurement ramp should be long enough that the size of the hysteresis loop is equal to that of the infinite duration limit. To check this, we show data in Fig. 2 for a sample of 100 $\mu$m glass spheres in mineral oil at $\phi = 0.56$, which is a stable sample over long time periods because the oil does not evaporate. Viscosity curves shown were taken first with a decreasing stress ramp followed by an increasing stress ramp for several different ramp durations. Since the control is a logarithmic ramp in stress over 4 decades, the measurement duration is specified in terms of duration per decade of stress. The hysteresis effect is characterized by the average ratio between the upper and lower branches of the hysteresis loop in $\eta(\tau)$ on a log-log scale. This is calculated equivalently as the geometric mean of viscosity ratio $\langle\eta_-(\tau)/\eta_+(\tau)]\rangle_g$ where $\eta_-$ and $\eta_+$ are viscosities for decreasing and increasing stress ramps, respectively, and $\langle ...\rangle_g$ indicates a geometric mean, i.e. averaged on a log-log scale. This average was done over the stress range of 0.1 to 8 Pa in the shear thickening regime. The hysteresis initially decreases with increasing measurement duration, then levels off for long measurements indicating a steady state limit. The initial duration-dependent behavior is characteristic of a transient relaxation, and the crossover between the regimes indicates a characteristic timescale for the sample to reach steady state. The leveling off of the viscosity ratio at a value of 1 suggests that in this case there is not a true hysteresis effect. At packing fractions very close to the jamming transition we sometimes find some non-zero hysteresis loop even for very long measurements, such that different steady states can be reached dependent on the shear history. The steady state viscosity curves we report are generally in the long-duration regime where the viscosity ratio has converged to a value near 1, for this sample we typically use a control ramp rate of 500 s per decade of stress. For each steady state measurement, we ramped the control parameter down then up at least once, but we show only one set of curves for brevity if they were all identical within typical variations of 10-20% from run to run.

# 4 Inertial scalings

In this section we show some examples of viscosity curves for suspensions at different packing fractions. While there are already many examples of the packing fraction dependence, here we vary the liquid viscosity and the packing fraction from near the jamming transition all the way down to zero to connect to hydrodynamic scalings that apply for suspensions at low concentrations and to quantify the importance of inertia in shear thickening.

We first show measurements of cornstarch suspended in water. These measurements were made with the Couette geometry. Viscosity is plotted vs. shear stress for several packing fractions in Fig. 3a. Apparent shear thickening is seen as regions with a positive slope of the viscosity curve for all packing fractions. For pure liquids this can be quantified in terms of a dimensionless Reynolds number, which represents a ratio of inertial to viscous stresses. This Reynolds number is usually of the form $\rho_l d^2\dot{\gamma}/\eta_l$ for pure liquids where $\rho_l$ and $\eta_l$ are the density and dynamic viscosity of the liquid, respectively. Thus, for the pure liquid the transition from a viscous-dominated regime with a nearly constant viscosity to an inertia-dominated regime with apparent shear thickening occurs at a fixed shear rate. However, we find that the sharp transition does not occur at the same shear rate for different packing fractions; specifically for low packing fractions the onset shear rate increases with packing fraction. The contribution of viscous

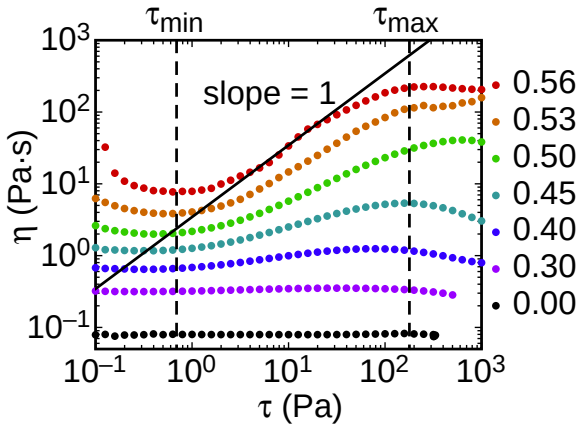


Figure 4: Viscosity curves for cornstarch in a glycerol-water mixture in which the Reynolds number remains small. Mass fractions $\phi_m$ are shown in the key; higher curves correspond to larger $\phi_m$. The solid line of slope 1 corresponds to a constant shear rate and the steepest possible steady state viscosity curve. The vertical dashed lines define the stress scales $\tau_{min}$ and $\tau_{max}$ that bound the shear thickening regime.

stresses to the viscosity of dense suspensions is much higher than that of the pure liquid (Brady and Bossis, 1985), so the viscous term in the denominator of the Reynolds number should be modified for suspensions. For the contribution of viscous stresses to suspension viscosity we do not take the zero shear rate limit of the viscosity since in this limit suspensions rheology can be dominated by non-viscous particle interactions (Barnes, 1989; Maranzano and Wagner, 2001a; Brown et al., 2010a), which results in shear thinning at low shear rates. Rather, we take as our best estimate the minimum suspension viscosity $\eta_m$ which occurs at the onset of shear thickening for each packing fraction. Our suspension Reynolds number is then $Re = \rho_l \dot{\gamma} d^2/\eta_m$.

In Fig. 3b we plot the shear stress normalized by $\eta_m\dot{\gamma}$ (corresponding to the viscous contribution to the stress) vs. suspension Reynolds number $Re$. With this normalization, data for any Newtonian fluid should collapse onto the same curve, which is nearly flat at low $Re$ in the viscous regime and transitions to a more positive slope at higher $Re$ due to inertial effects. We find that the lower mass fractions $\phi_m \lesssim 0.4$ indeed collapse onto a single curve. The very mild increase in effective viscosity for $1 \lesssim Re \lesssim 100$ is typical of hydrodynamic flows in this range of $Re$ where viscous stresses are dominant but inertial effects start to become measurable (Schlichting, 1960). Inertial models for shear thickening typically produce similar mild shear thickening effects in the range $0.1 \lesssim Re \lesssim 100$ (Kulkarmi and Morris , 2008). The approximate scaling $\tau \sim \dot{\gamma}^{3/2}$ for $100 \lesssim Re \lesssim 3000$ as inertia becomes stronger is also typical (Donnelly and Simon, 1960). The asymptotic scaling $\tau \sim \rho\dot{\gamma}^2 d^2$ expected in the fully inertial regime is often not found until $Re \gtrsim 10^3$ (Schlichting, 1960). The data collapse for $\phi_m \lesssim 0.4$ suggests that in this regime the suspension behaves like a Newtonian fluid. In contrast, for $\phi_m \gtrsim 0.4$ the normalized viscosity curves deviate significantly from this scaling, increasing more steeply than inertial stresses are expected to be able to grow, and the steep shear thickening onsets at much lower values of $Re$. The onset of shear thickening occurs at *lower* shear rates for larger $\phi$, instead of the *higher* shear rates which would be required before inertial stresses dominate over viscous stresses. Instead, the onset appears to be set by a constant stress scale.[3]. This suggests that inertial stresses are relatively small in this regime where shear thickening becomes more dramatic. This does not necessarily imply that viscous forces are dominant in the system, rather the lack of data collapse for $\phi_m \gtrsim 0.4$ in Fig. 3 suggests other stresses must be involved. We will show in Sec. 7 that friction is the dominant mechanism of stress transfer at high packing fractions.

The scaling seen in Fig. 3 suggests two competing mechanisms for different types of shear thickening – inertial and Discontinuous – such that only the stronger effect is observed in a single viscosity curve. To obtain a system where the Reynolds number remains low in the Discontinuous Shear Thickening stress range even at low packing fractions, a liquid of higher viscosity can be used. Accordingly, we suspended cornstarch in a glycerol-water mixture with a viscosity 80 times that of water. The viscosity curves vs. stress for different packing fractions can be seen in Fig. 4. Comparing with the data for cornstarch in water in Fig. 3, we can see that there is similar strong shear thickening at high packing fractions, but no apparent shear thickening at low packing fractions. At the same stress, the Reynolds number is lower by about a factor of $\eta_l^2 \approx 600$ for the suspension with glycerol, thus $Re < 100$ and inertial effects

[3]For $\phi_m \gtrsim 0.4$, $\eta_m$ is likely an overestimate of the viscous contribution to viscosity as the non-Newtonian terms become larger near the jamming transition and $\eta_m$ likely represents a cross-over between the shear thinning and shear thickening effects (Brown et al., 2010a) Regardless, since the viscous contribution to the viscosity increases while the onset shear rate decreases with packing fraction, the onset Reynolds number still becomes very low at high packing fractions.

remain negligible in the stress range of Discontinuous Shear Thickening even in the limit of zero packing fraction. We can see the remaining shear thickening uncontaminated by inertial effects is now very weak at $\phi_m = 0.40$, and is almost imperceptible at $\phi_m = 0.30$. This is a typical example of Discontinuous Shear Thickening, in which the region with positive slope of $\eta(\tau)$ occurs in a stress range that is nearly independent of packing fraction. This slope increases with packing fraction, approaching $\eta \sim \tau$ (solid line in Fig. 4) corresponding to a discontinuous stress/shear-rate relation. The bounds of the shear thickening regime are characterized on the lower end by $\tau_{min}$ defined as the onset of a positive slope of $\eta(\tau)$, and on the upper end by $\tau_{max}$ defined as the transition from positive to negative slope. These transitions are measured as the crossover between local power law fits on either side. Because of fluctuations typically on the scale of 10-20% in the viscosity we do not count any features smaller than that threshold as distinct transitions. Section 5 is devoted to determining the scaling for $\tau_{min}$, and Secs. 7 to 10 are devoted to determining the scaling and mechanism for $\tau_{max}$.

There are several other dimensionless numbers that have been used to describe inertial effects in particulate flows. In particular, often the system size $d$ is replaced with the particle size $a$, for example leading to a Bagnold number (Bagnold, 1954). The distinction between the two types of scalings can be made with a pure liquid at zero packing fraction which has the system size scale of $d$ but no particle length scale. Since the cornstarch-in-water data for $\phi_m \lesssim 0.4$, including $\phi_m = 0$, collapse based on a Reynolds number scaling in terms of $d$, the system size should be taken as the relevant length scale as is typical in pure fluids, and no other dimensionless inertial number would collapse the data over as wide a range. Since the Reynolds number scaling comes from pure liquids, it appears that the global steady state viscosity of suspensions can be described by Newtonian hydrodynamics up to $\phi_m \approx 0.4$, and possibly higher in larger systems where inertial effects are stronger. At higher packing fractions, strong shear thickening can be seen at lower shear rates which may overwhelm inertial effects. We can qualitatively distinguish high-$Re$ flow from Discontinuous Shear Thickening because the packing fraction, shear rate, liquid viscosity, and gap size dependence of high-$Re$ flows differs from that of Discontinuous Shear Thickening, and the steepest possible scaling for inertial flows is $\tau \sim \dot{\gamma}^2$ in the limit of large shear rates (Bagnold, 1954). Since the focus of this paper is on Discontinuous Shear Thickening, all of the following data will be in the high packing fraction regime ($\phi_m \gtrsim 0.4$) and for $Re < 100$ to avoid mixing inertial effects with Discontinuous Shear Thickening.

# 5 Gravity and the onset stress

Suspensions and colloids occupy a region of phase space where many physical forces may be relevant; these include Brownian motion, gravity, surface tension, and electrostatics. One consequence of this is that there are different scaling laws for the onset of shear thickening in different parameter regimes where one of these forces is dominant (Hoffman, 1998; Maranzano and Wagner, 2001a,b; Bergenholtz et al., 2002; Shenoy and Wagner, 2005; Brown et al., 2010a). Here we address the case of a gravity-dominated regime. This regime is not yet as well-characterized as the other regimes, but an understanding of the effects of gravity on the onset stress will make it possible to further generalize the conditions for the onset of shear thickening with a mechanism that accommodates all of these scalings.

We measured steady state viscosity curves for a series of suspensions of glass spheres ($\rho = 2.46$ g/mL) with diameters ranging from 6 to 2000 $\mu$m in diameter in either mineral oil ($\rho = 0.88$ g/mL) or water ($\rho = 1.00$ g/mL) at packing fractions ranging from 0.50 to 0.58 These particles are large enough to settle over time since the glass is much denser than the liquids. In each case, the major features were qualitatively similar to Fig. 4, with increasingly steep slopes at higher packing fractions and shear thickening occurring in a relatively fixed stress range. We obtained mean values of $\tau_{min}$, corresponding to the onset of a positive slope of $\eta(\tau)$, for each suspension averaged over a range of packing fractions close to but below $\phi_c$. The mean values of $\tau_{min}$ for each particle size are plotted in Fig. 5.

For the largest particles with $a \geq 500$ $\mu$m, the suspensions would not remain confined between the rheometer plates with a vertical boundary because the particles are so heavy that they can no longer be confined by surface tension. Since this confinement is set by the interplay between gravitational and surface tension forces, it is no surprise that loss of confinement occurs for particles on the order of the capillary length, or $\sim 1$ mm. We could still make measurements with some sample extended outside the area between the plates to obtain the scales of $\tau_{min}$ and $\tau_{max}$. For the largest glass beads with a diameter of 2000 $\mu$m, we found no shear thickening regime. The significance of this maximum particle size for shear thickening will be discussed in Sec 11.

It can be seen in Fig. 5 that there are two distinct scaling regimes which meet at a minimum near a particle size of 50 $\mu$m. For smaller particles with $a \leq 50$ $\mu$m that approach the colloidal regime, interparticle interactions from various sources including electrostatics and Brownian motion tend to become large relative to gravity and can affect the onset stress. For example, a high particle-liquid surface tension can result in an effective attraction between particles which can form force chains that span the system and jam it. This in turn results in a yield stress and shear thinning even at low packing fractions which then can hide shear thickening (Brown et al., 2010a). Specifically for this measurement series, with glass beads 50 $\mu$m and larger, the particles will disperse well and shear thicken in either oil or water. However, the 6 $\mu$m glass particles are effectively hydrophilic. Consequently in oil they have a

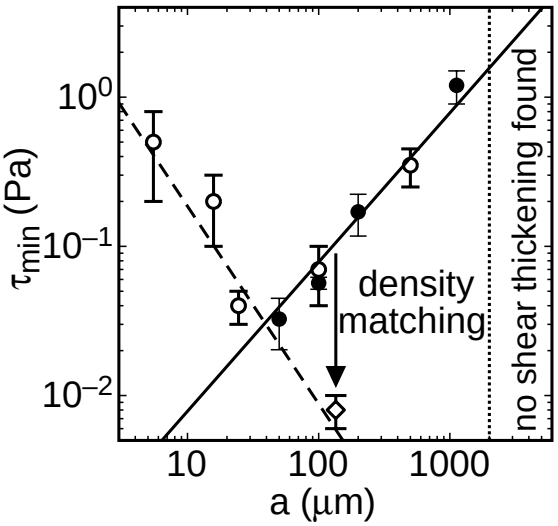


Figure 5: The stress at the onset of shear thickening $\tau_{min}$ for glass spheres of different diameters $a$ in mineral oil (solid circles, $\Delta\rho = 1.58$ g/mL) or water (open circles, $\Delta\rho = 1.46$ g/mL). Open diamond: polyethylene in silicone oil ($\Delta\rho \approx 0.0001$ g/mL). The solid line is the shear stress required to lift particles off the top layer of the packing against friction and gravity $\mu_{eff}\Delta\rho ga/15.3$. Dashed line: representative curve for data where gravity is not the dominant interparticle interaction. Dotted line: bound above which larger particles did not exhibit any shear thickening regime.

significant yield stress and shear thickening was not observed at all. We will revisit the issue of other scaling regimes for the onset stress for small particles in Sec. 11.

To understand the scaling of $\tau_{min}$ for the larger particles with $a \geq 50$ $\mu$m, we now analyze the effects of gravity on non-Brownian suspensions. In the absence of shear, gravity results in particles settling and resting on the bottom plate. The measured stress would come only from shear of the thin fluid layer on top of the settled particles. The drag force from the shear in the liquid layer above the particles can start to move the upper layer of particles if it exceeds the static frictional force between particles under gravity. In a parallel plate geometry, the horizontal cross-section has a uniform area so, to balance forces, the shear stress $\tau$ must be on average independent of height. As an estimate for the drag force on a particle in the top layer, we use the drag force on a sphere sitting on a flat surface is $2.55\pi\tau a^2$ (Goldman et al., 1967). The frictional force on one of these particles is $\pi\mu_{eff}\Delta\rho g a^3/6$ for an effective static coefficient of friction $\mu_{eff}$, density difference $\Delta\rho$ between the particles and liquid, and acceleration of gravity $g$. Since the particles are sitting on a pile of beads instead of a flat surface, the effective friction is enhanced by geometry because of the need for the spheres to rise over the particles in the layer below. To measure $\mu_{eff}$, we glued 1 mm glass beads in a monolayer to a glass slide. We then performed an inclined plane test with this system immersed in water, setting individual glass beads on top of the bead-covered slide and slowly tilting the slide until the loose beads started falling down. From this we obtained $\mu_{eff} = 0.8 \pm 0.1$. Balancing the drag and frictional forces gives the stress at the onset of granular shear to be $\mu_{eff}\Delta\rho ga/15.3$. This prediction is plotted in Fig. 5. It is seen to match well the measured onset stress $\tau_{min}$ for particles between 50 and 1125 $\mu$m in diameter. This confirms that the onset of shear thickening in the gravity-dominated regime is set by the stress required to initiate shear of the particles against gravity and friction.

Since the onset scaling for large particles is set by gravity, this suggests $\tau_{min}$ can be lowered by density matching. We tested this by measuring steady state viscosity curves for 100 $\mu$m polyethylene particles in silicone oil with a density difference of about $10^{-4}$ g/mL. The mean value of $\tau_{min}$ is shown in Fig. 5 by the open diamond. While $\Delta\rho$ was reduced by a factor of $10^4$ compared to the non-density matched case, the onset stress was only reduced by an order of magnitude. In this case the density-matched data fall onto a similar scaling as was found for the glass for $a \leq 25$ $\mu$m. In many cases for particles even as large as 100 $\mu$m, density matching can have no effect on the onset stress due to the significance of interparticle interactions. For cornstarch in water, density matching by adding CsCl to the water did not reduce the onset stress. For glass spheres in a heavy liquid $\rho = 2.46$ g/mL (Cargille labs inorganic salt series) we found no measurable decrease in the onset stress compared to mineral oil or water, and found shear thinning below the onset as opposed to the Newtonian behavior found for glass suspensions whose onset is determined by the gravitational scaling (Brown and Jaeger, 2009; Brown et al., 2010a). This suggests that in each

of these cases, the stress scale characterizing interparticle interactions which is dominant for smaller particles is very close to the onset stress if not the dominant factor. These results show that while density matching can lower the onset stress in the gravity-dominated regime, it cannot do so beyond the limits set by any other stress scales due to particle interactions. Thus we generally expect a larger effect of density matching for very large particles further into the gravity dominated regime.

In this set of experiments with a parallel plate setup, gravity caused particles to settle and initiating shear required exceeding the hydrostatic pressure of the top layer of particles only. In contrast, in a Couette cell with vertical walls a yield stress was found that scales with the hydrostatic pressure due to the full weight of the grains in the suspension pushing on the walls (Fall et al., 2009). We know that such a yield stress can hide shear thickening if it is larger than the stress from shear thickening mechanisms (Brown et al., 2010a). This implies that the effect of the yield stress from gravity is shear-geometry dependent because of the directionality of gravity. While this yield stress can hide shear thickening effects and move the onset (Brown et al., 2010a), there is no indication that the shear thickening mechanism itself is geometry dependent. Thus a horizontal rheometer plate allowed for the observation of shear thickening in suspensions of large particles without it being hidden by a yield stress.

# 6 Shear profile

We next show shear profile measurements of both density matched and non-density-matched suspensions that exhibit Discontinuous Shear Thickening to obtain constitutive relations in the shear thickening regime. We will show that gravity plays a dominant role in determining the shear profile in the suspension regime. However, to account for the stress jump in the Discontinuous Shear Thickening regime, a non-local stress term independent of local shear rate and height will be required.

To measure the shear profile we used a video camera with a bellows and magnifying lens to obtain a pixel size as small as 10 $\mu$m. The camera was placed next to the standard parallel plate rheometer setup and focused on the outer edge of the sample in the plane of the shear direction and shear gradient. While there is some distortion from looking through the curved liquid-air interface, we can track individual particle motions to measure the shear profile at the edge of the sample. Videos were taken for constant shear rate conditions after the steady state was reached. Steady state shear profiles obtained by averaging the velocities at each height. A small tilt of the camera caused a smoothing effect over about 4% in the depth.

We first describe results for a settling suspension of 150 $\mu$m $ZrO_2$ spheres in mineral oil at $\phi = 0.53$ with a gap $d = 890$ $\mu$m. This suspension is chosen for visualizations instead of glass because the particles are opaque. The raw particle motions under shear are shown in supplementary videos 1 and 2 for two different shear rates. Local velocities are obtained by particle image velocimetry. Velocity profiles are shown in Fig. 6a for a range of shear stresses. The corresponding viscosity curve is shown in Fig. 6b. Below $\tau_{min} \approx 0.3$ Pa, we found no measurable particle motion up to a resolution of $10^{-3}$ times the plate displacement. In this regime the particles remained settled due to gravity as expected based on the measurements of $\tau_{min}$ in Sec. 5. Above the onset, we found a narrow shear band near the moving top plate. This also agrees well with the observations that the onset of shear thickening corresponds to the onset of dilation (Metzner and Whitlock, 1958), since shearing of the grains is what results in dilation. The width of the shear band increased as the stress was increased. Layering was clearly observed at higher shear rates. Effects of this layering on the measured stress can be observed for suspensions that are a few layers thick, where the layering can be frustrated at gap sizes corresponding to non-integer particle widths corresponding to higher stresses, but this contribution to the stress becomes negligible for gaps larger than about 5 layers (Brown et al., 2010b). We performed similar measurements with glass particles in mineral oil with a gap 12 particles wide as opposed to 6 particles with the $ZrO_2$. Results were qualitatively similar to the $ZrO_2$ data, although layering was less prominent, appearing only clearly in the top two layers, as expected for a finite-size effect.

We next describe results for nearly density-matched 135 $\mu$m polyethylene spheres in silicone oil at $\phi = 0.55$ with a gap 850 $\mu$m wide. The lighting used to take the videos heated the silicone oil by several degrees, so there was a slight density difference of about $\Delta\rho = -0.01$ g/mL such that the particles were slightly buoyant, effectively reversing the direction of gravity. Because the smaller density difference moves the onset of shear thickening to very low shear rates, we did not obtain measurements of the shear profile below $\tau_{min} \approx 0.01$ Pa. Velocity profiles are shown in Fig. 7a for a range of shear stresses. The corresponding viscosity curve is shown in Fig. 7b. In the shear thickening regime, the velocity gradient in the bulk was relatively small, with a shear band at the bottom plate and a layered structure at the top plate. In this case, the shear band appeared at the bottom plate and the direction of curvature of the shear profile was reversed due to the inversion of gravity. The shear band widened at higher stresses, similar to the case for the settling $ZrO_2$. Interestingly, for all three suspensions the layering was most pronounced near the top moving plate despite the gravity inversion.

These measurements also allow us to measure slip directly. When the particles were settled with the plate moving past, there was not even contact so the difference between plate and particle motions is technically not slip and

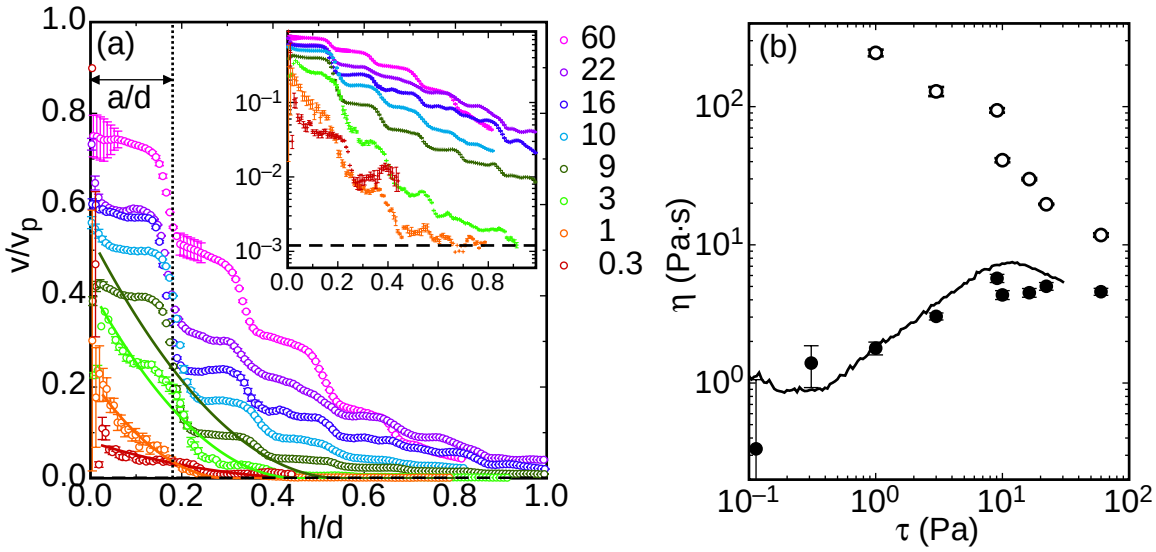


Figure 6: (a) Shear profiles at the plate edge for settling particles of $ZrO_2$ in mineral oil ($\Delta\rho = 2.9$ g/mL). The mean velocity $v$ is normalized by the plate edge velocity $v_p$, and the depth $h$ is normalized by the gap $d$. Shear stress $\tau$ for each profile shown in the key; higher curves correspond to larger $\tau$. Dashed line: upper bound of $10^{-3}$ for a measurement at $\tau < \tau_{min}$. Dotted black line: depth equal to 1 particle diameter. Solid lines: fits of Eq. 5 to the data for $\tau < \tau_{max}$. Inset: same data on log-linear scale. (b) Local viscosity curves based on the local shear rate from the shear profile. Open circles: local viscosity in bulk region. Solid circles: local viscosity in the shear band near the top plate. Solid line: global viscosity curve.

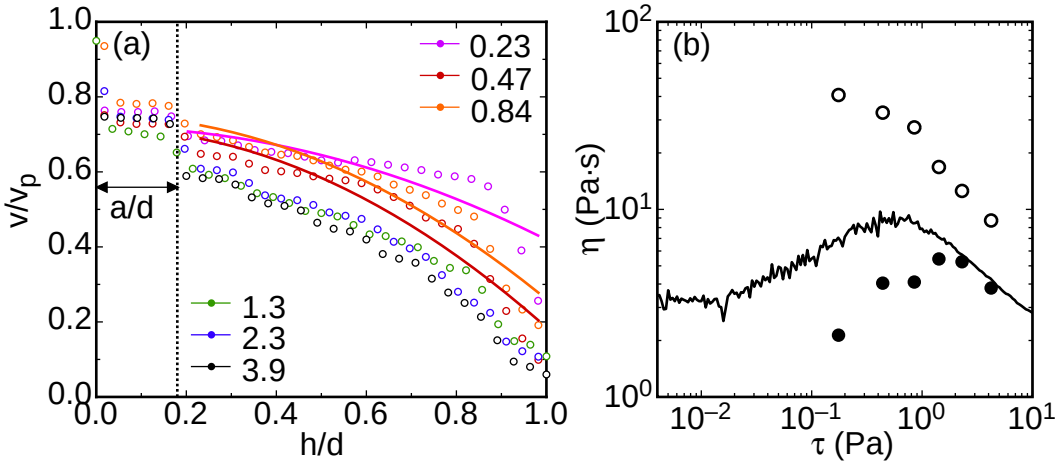


Figure 7: (a) Shear profiles at the plate edge for density matched polyethylene in silicone oil ($\Delta\rho \approx -0.01$ g/mL). The mean velocity $v$ is normalized by the plate edge velocity $v_p$, and the depth $h$ is normalized by the gap $d$. Shear stress $\tau$ for each profile shown in the key; lower curves correspond to larger $\tau$. Dotted black line: depth equal to 1 particle diameter. Solid lines: fits of Eq. 6 to the data for $\tau < \tau_{max}$ with the substitution $h/d \to 1 - h/d$ since the particles are lighter than the liquid. (b) Local viscosity curves based on the local shear rate from the shear profile. Open circles: local viscosity in bulk region. Solid circles: local viscosity in the shear band near the bottom plate. Solid line: global viscosity curve.

should not be expected to follow slip correction models which usually assume a linear bulk velocity profile. Settling and slip effects can be distinguished by comparing to the density matched case shown in Fig. 7a where the settling rate is much lower than the shear rate for all of the data shown. The difference between the speed of the top plate and neighboring particles in the more developed flow regimes is around 25%, roughly independent of shear stress. This does not change significantly at the boundary between shear thickening and shear thinning regimes, confirming that those rheological boundaries are not determined by slip. Since the goal of this paper is to understand the global response of Discontinuous Shear Thickening, we do not 'correct' for slip. In any case, making a correction for slip does not significantly alter the shape of the viscosity curves nor move the regime boundaries in terms of stress because it only affects the shear rate. While it does slightly shift the magnitude of the viscosities reported, we do not make any conclusions based on the magnitude of the viscosity. The lack of contact between the particles and plate with settling is not problematic in terms of the mechanical response because viscous interactions within the liquid transmit stress between them just as well as hard contacts. This is confirmed by our observation that switching from smooth to rough plates does not change the stress scales or qualitative response.

## 6.1 Local constitutive relations and the shear profile

Here we consider the significance of the shape of the shear profile in the shear thickening regime. Since the shear stress in a parallel plate geometry is independent of height, a local hydrodynamic constitutive relation $\tau(\dot{\gamma}_l)$ dependent on a local shear rate $\dot{\gamma}_l$ would correspond to a linear velocity profile. To account for a non-linear steady state velocity profile, fixes have been introduced in the past to make local constitutive relations self-consistent by relating fluctuations in the local shear rate to an effective kinetic temperature (Nott and Brady, 1994; Bocquet et al., 2001) and by including the effect of the local variation in packing fraction on the viscosity (Nott and Brady, 1994; Bocquet et al., 2001; Fall et al., 2010). In granular shear flows, the initial inhomogeneity is usually attributed to dilation near the moving plate (Mueth et al., 2000).

Rather, we suggest that here gravity and friction are responsible for curvature in the shear profile, as in sedimenting flows (Lenoble et al., 2005). Specifically, there can be frictional forces between particles due to the weight of the packing which increases with depth $h$ into the sample relative to the top plate (for downward gravity) if the particles remain in contact via force chains. A non-linear shear profile could be the result of such an explicit height-dependence. The simplest form for a local stress relation that includes gravity is

$$\tau = \eta_\nu \dot{\gamma}_l + \tau_g h/d + \tau_c \tag{3}$$

where $\eta_\nu$ is the viscous hydrodynamic contribution to the visocsity, the gravitational stress scale $\tau_g \equiv \mu_{eff}\Delta\rho g d/15.3$ from Sec. 5, and $\tau_c$ represents any stresses that are independent of local shear rate and depth such as interparticle attractions. Rearranging gives the local shear rate

$$\dot{\gamma}_l = (\tau - \tau_c - \tau_g h/d)/\eta_\nu \ . \tag{4}$$

This implies a critical depth $h_c/d = (\tau - \tau_c)/\tau_g$ at which the shear rate equals zero and beyond which there is no shearing of grains. This suggests the shear stress must exceed the sum of interparticle stresses ($\tau_c$) and gravitational stress on the first layer of particles ($\tau_g a/d$) to shear grains, the same condition for the onset of shear thickening shown in Fig. 5. The velocity profile can be obtained by integrating the local shear rate from Eq. 4 over depth. There are two solution regimes:
if $h_c < d$, then

$$\frac{v}{v_p} = \frac{\tau_g}{2\tau_\nu}\left(\frac{h_c - h}{d}\right)^2 \ , \tag{5}$$

and if $h_c > d$, then

$$\frac{v}{v_p} = \frac{\tau - \tau_c - \tau_g}{\tau_\nu}\left(\frac{d-h}{d}\right) + \frac{\tau_g}{2\tau_\nu}\left(\frac{d-h}{d}\right)^2 \tag{6}$$

where the plate velocity $v_p = d\dot{\gamma}$ and the viscous stress scale is defined by $\tau_\nu \equiv \eta_\nu \dot{\gamma}$. The curvature of the velocity profile characterized by a quadratic term is set by the ratio of gravitational to viscous stresses $\tau_g/\tau_\nu$. The velocity profile becomes linear in the limit where this ratio goes to zero ($h_c > d$) as expected. These profiles are concave up, and become more linear with increasing $\tau$ in qualitative agreement with the data in Fig. 6a. The equations were written for the case where the effective gravity on the particles is downward. For the polyethylene data where the effective gravity is upward, we have to make the substitution $h/d \to 1 - h/d$ which reverses the concavity.

Because we are applying a continuum model to a system that is quantized due to layering, and fluctuations could smooth out mean shear profiles, we do not expect the gravitational model to be exact. Rather, the purpose is to determine how relevant gravity is to the shear profile. To test this model, we fit the function

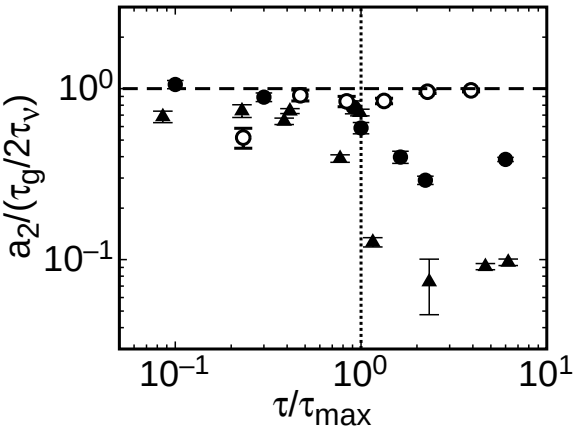


Figure 8: Quadratic curvature $a_2$ of velocity profiles normalized by the model prediction from Eq. 6 with $\tau_{min}$ used as an estimate for the viscous stress $\tau_\nu$. The curvature $a_2$ is obtained from fitting Eq. 7. Data is fit for different normalized shear stresses $\tau/\tau_{max}$ for glass in mineral oil (solid triangles, $\Delta\rho = 1.58$ g/mL), polyethelyne in silicone oil (open circles, $\Delta\rho = -0.01$ g/mL), and $ZrO_2$ in mineral oil (solid circles, $\Delta\rho = 2.9$ g/mL). The data collapse close to a value of 1 for $\tau < \tau_{max}$ suggests the curvature of the shear profile is due to the weight of the particles on deeper layers which is transferred via frictional contacts, and that the contribution of viscous stresses to the viscosity does not increase significantly in the shear thickening regime.

$$v/v_p = a_1 \frac{(h_c - h)}{d} + a_2 \left[\frac{(h_c - h)}{d}\right]^2 \tag{7}$$

to the measured velocity profiles for each shear rate. Some of these fits are shown in Figs. 6a and 7a. For $ZrO_2$ and glass, it appears that $h_c < d$ for $\tau < \tau_{max}$ so we fix $a_1 = 0$ according to Eq. 5. The quadratic coefficient $a_2$ can be compared to the prediction of Eqns. 5 and 6 with an estimate for the viscous stress $\tau_\nu$. We showed in Sec. 5 that at the onset of shear thickening the viscous stress must be just enough to initiate shear so $\tau_\nu \approx \tau_{min}$. Since the shear rate increases slowly in the shear thickening regime for Discontinuous Shear Thickening, we will use this estimate for the entire shear thickening regime. The measured curvature $a_2$ normalized by the predicted value $\tau_g/2\tau_{min}$ is plotted in Fig. 8 for each fit for $ZrO_2$, polyethylene, and glass. For $\tau < \tau_{max}$, the data for all three density differences collapse onto a single curve with $a_2/(\tau_g/2\tau_{min}) \approx 1$. This value is in agreement with the model which confirms the curvature of the shear profile is set by a balance of gravity-induced friction and viscous interactions. Because the data collapse works reasonably well for systems of different sizes, it rules out the role of finite size effects in setting the velocity profile curvature.

The shear profile measurements are consistent with the argument from Sec. 5 that the onset of shear thickening corresponds to the onset of granular shear, and at lower shear stresses particles remain settled due to gravity or held together by other interparticle forces. In the shear thickening regime, the curvature of the shear profile suggests a balance between gravity-induced friction and viscous interactions, but this can only hold if the weight of the packing builds up in deeper layers. This implies force chains between particles must extend from plate to plate, which is a common feature of granular systems. The quadratic shear profile requires a balance between gravity-induced friction and viscous forces so is specific to suspensions within this model. The collapse of the data in Fig. 8 in the shear thickening regime onto a nearly constant value also suggests that the contribution of viscous stresses to the viscosity is not increasing in the shear thickening regime, in contrast to the expectations of hydrodynamic models for shear thickening. In Sec. 7 we will show that the increase in viscosity in the shear thickening regime comes from normal stresses which are transmitted along the same frictional contacts that transmit gravitational forces.

For $\tau > \tau_{max}$, the different curvature values do not collapse onto a single curve, suggesting either that the model fails in this regime or at least that $\tau_{min}$ is no longer a good approximation of $\tau_\nu$ in this regime. Rather, the profiles appear to be closer to exponential (see inset of Fig. 6a), similar to granular shear profiles of spherical particles (Mueth et al., 2000). This suggests that above $\tau_{max}$ the shear profile could be that of a fully granular system where there is no need for a contribution of viscous hydrodynamics.

An alternate model attributes curvature in the shear profile to variations in the local packing fraction (Fall et al., 2010). In this model the small changes in packing fraction from dilation and viscous resuspension are significant because the viscosity divergence with packing fraction comes from the viscous lubrication layer goes to zero at the

jamming transition. However, our results on the curvature of the shear profile suggest stress is transmitted mostly through frictional contacts rather than viscous interactions. Since the strong packing fraction dependence of the viscous hydrodynamic part of the viscosity depends on lubrication layers between particles, it should not apply when there are frictional contacts, and thus the curvature can be explained without the need to account for local packing fraction variation. There are other reasons to suspect a hydrodynamic model would not account for the measured stresses in the shear thickening regime. Since dilation *reduces* the average packing fraction in the shear thickening regime, it should result in a *lower* viscosity in a hydrodynamic model. Additionally, since viscosity values measured are up to $10^7$ times the solvent viscosity (Brown and Jaeger, 2009), this would require subatomic gaps in a lubrication model. However, lubrication in molecular liquids breaks down at 2 molecular layers, below which the liquid is frictional (Van Alsten & Granick, 1988). These issues suggest the stresses in the shear thickening regime must be explained by some non-viscous mechanism.

Another model attributes curvature in the shear profile to a gradient in the kinetic energy of the particles (Nott and Brady, 1994; Bocquet et al., 2001). The contribution of this effect to the local stress gradient can be estimated as $\nabla\tau \sim \rho v \nabla v \sim \rho\dot{\gamma}^2 d$ using the observation that the scale of the rms fluctuations in velocity are comparable to the mean flow velocity in granular flows with solid particle contacts (Bocquet et al., 2001). This contribution to the stress gradient is at most on the order of $10^{-4}$ times the gravitational contribution to the stress gradient $\nabla\tau \sim \Delta\rho g$ even at the maximum stress in the shear thickening regime for the measurements shown in Figs. 6a and 7a. Thus we expect the contribution of the kinetic energy to the shear profile to be negligible in the regime of our measurements.

## 6.2 Localized viscosity curves

While we found changes in the shear profile at the transitions between shear thinning and shear thickening at $\tau_{min}$ and $\tau_{max}$, the remarkable feature of Discontinuous Shear Thickening is the large stress jump. The collapse of the curvature values in Fig. 8 for $\tau < \tau_{max}$ suggests the viscous term $\eta_\nu\dot{\gamma}$ is nearly constant in the shear thickening regime, so the stress jump can not be attributed to viscous interactions. Instead, the stress jump must be hidden within the uniform stress term $\tau_c$, which we will show is due to frictional interactions in Sec. 7. This implies that while yield stress effects from gravity are directly seen in the shear profile, the curvature and inhomogenieties in the shear profile are not directly related to the stresses responsible for shear thickening. Other experiments have found a shear profile in the Discontinuous Shear Thickening regime corresponding to plug flow (Maranzano and Wagner, 2001a). The variety of observed shear profiles reinforces the conclusion that the shear profile is not directly related to the stresses responsible for Discontinuous Shear Thickening $\tau_c$, rather the shear profile is mostly determined by lesser contributions to stresses.

A similar issue with local constitutive relations appears if we use the local velocity profile to obtain local viscosity curves. The local viscosity can be calculated as the ratio of the measured global stress and the local shear rate from the derivative of the velocity profile. To separate the bulk region from the shear band regions we use the mean slope of the velocity profile over different ranges of depth. For the profiles in Fig. 6a we use the range $0.25 < h/d < 0.8$ for the bulk, and $h/d < 0.3$ for the shear band at the top plate. For the profiles in Fig. 7a we use the range $0.2 < h/d < 0.8$ for the bulk, and $h/d > 0.85$ for the shear band at the bottom plate. According to the model of Eq. 6, the local bulk viscosities roughly approximate the linear term, which corresponds to the viscous contribution to the viscosity. These local viscosities are plotted in Fig. 6b and 7b, respectively, along with the global viscosity curves. For each suspension, the shear band shows shear thickening similar to the global curve, while the bulk region appears to be everywhere shear thinning based on the local viscosity. In the non-density matched case below $\tau_{min}$, the bulk was observed to be settled (i.e. locally jammed), corresponding to an infinite local viscosity. Thus the bulk region appears to behave like a yield stress fluid with shear thinning but no shear thickening. The region that qualitatively determines the global rheology is not the bulk but rather the near-wall region where the shearing occurs. This is not surprising from a granular or solid mechanics point of view where the global behavior is often determined by the failure in the weakest region.

Another test of the validity of local constitutive equations comes from comparisons of measurements in different measuring geometries. For a measurement in a cone and plate geometry the mean shear rate is independent of radius because the plate speed is proportional to the gap height at each point along a radius, while in a parallel plate setup the mean shear rate increases with radius because the plate speed is faster near the edge but the gap remains the same. Thus, assuming a local constitutive relation between shear stress and rate holds, an apparent viscosity curve measured in a parallel plate rheometer should always be smoothed out compared to one measured in a cone and plate rheometer. However, a comparison of measurements of Discontinuous Shear Thickening in different geometries showed that the apparent viscosity curve from a parallel plate rheometer was *steeper* than that measured with a cone and plate rheometer (Fall et al., 2008). These problems with a local constitutive relation between shear stress and shear rate suggest the global response cannot be described by viscous stresses only. In the next section, it will be shown that the stresses in the Discontinuous Shear Thickening regime are mostly frictional, due to confining stresses described by a non-local constitutive relation that depends on the boundary conditions.

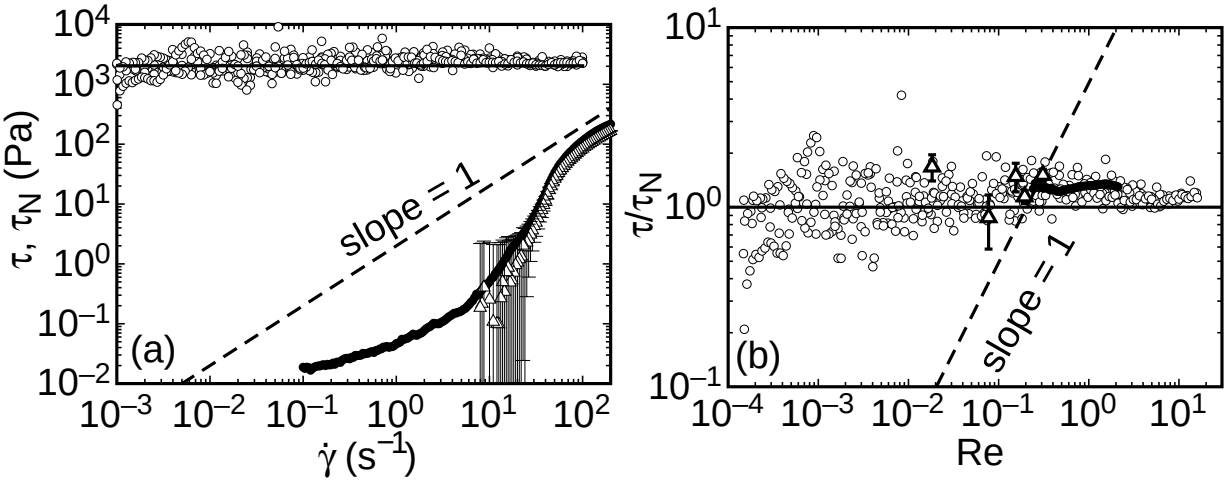


Figure 9: (a) A comparison of flow curves measured with different boundary conditions for glass spheres in water at $\phi = 0.52$ ($< \phi_c$). Solid circles: shear stress $\tau$ for 100 $\mu$m spheres in a fixed gap measurement with the standard parallel plate setup. Open triangles: normal stress $\tau_N$ from the same measurement. The absolute uncertainty on the normal stress is 2 Pa, so the normal stress cannot be resolved at the low end. Open circles: $\tau$ for 500 $\mu$m spheres with a fixed normal stress of 2040 Pa (solid line) in the modified parallel plate setup with a hard wall. Dashed line: slope 1 corresponding to a Newtonian scaling for reference. (b) Circles: same data with the shear stress $\tau$ normalized by normal stress $\tau_N$ vs. $Re = \rho d^2\dot{\gamma}/\eta_m$. Open triangles: constant shear rate measurements in the standard parallel plate setup in which the normal force was recalibrated before each measurement. Solid line: $\tau = \tau_N$ indicating a frictional scaling. Dashed line: $\tau = \eta_m\dot{\gamma}$ corresponding to a viscous scaling.

# 7 Normal forces and the boundary condition

(Schlichting)

In this section we use measurements of shear and normal stresses under different boundary conditions to show that the global mechanical response can be described by a solid frictional constitutive law rather than a viscous law.

## 7.1 Frictional scaling

Here we compare steady state viscosity curves along with normal stress measurements for similar suspensions with different boundary conditions. The sample was 100 $\mu$m diameter glass spheres in water at a packing fraction of $\phi = 0.52$ ($< \phi_c$). We first show results from a standard parallel plate setup (Fig. 1a) with a diameter of 50 mm which results in a better normal stress resolution than smaller plates. The shear stress $\tau$ and normal stress $\tau_N$ are shown in Fig. 9a as functions of shear rate $\dot{\gamma}$ for a measurement in which the gap size is fixed at 0.72 mm. The region with slope greater than 1 defines the shear thickening regime. We found positive normal stresses, corresponding to the sample pushing against the plates, in agreement with other measurements of Discontinuous Shear Thickening (Lootens et al., 2005; Fall et al., 2008). The shear and normal stresses track each other extremely well in functional form and magnitude. The cutoff of $\tau_N$ at the low end corresponds to the measurement dropping below the relative resolution of the normal stress of about 0.3 Pa.

We next used the walled rheometer setup without a liquid air interface as shown in Fig. 1b. In this case a sample of 500 $\mu$m glass spheres in water was used; the larger particles were necessary to avoid them escaping through the gap between the side wall and top plate. While the values of $\tau_{min}$ and $\tau_{max}$ differ with particle size (see Figs. 5, 17), otherwise the samples behave in a qualitatively similar way in the normal parallel plate setup. The normal force on the top plate was fixed at 1 N (2040 Pa), consequently the gap size was allowed to vary. The viscosity curve is shown in Fig. 9a. In contrast to the standard parallel plate setup, the rheology is that of a yield stress fluid with no shear thickening regime. Such a dramatic difference in behavior with a change in boundary conditions would be unexpected from a local hydrodynamic constitutive relation, and implies a non-local effect. The common feature of both measurements is the connection of the shear stress to the normal stress. We plot the ratio of stresses $\tau/\tau_N$ vs. the Reynolds number $Re = \rho_l d^2\dot{\gamma}/\eta_m$ for both measurements in Fig. 9b. Additionally, we show steady state values for measurements taken at constant shear rate in the shear thickening regime in which the normal force was recalibrated

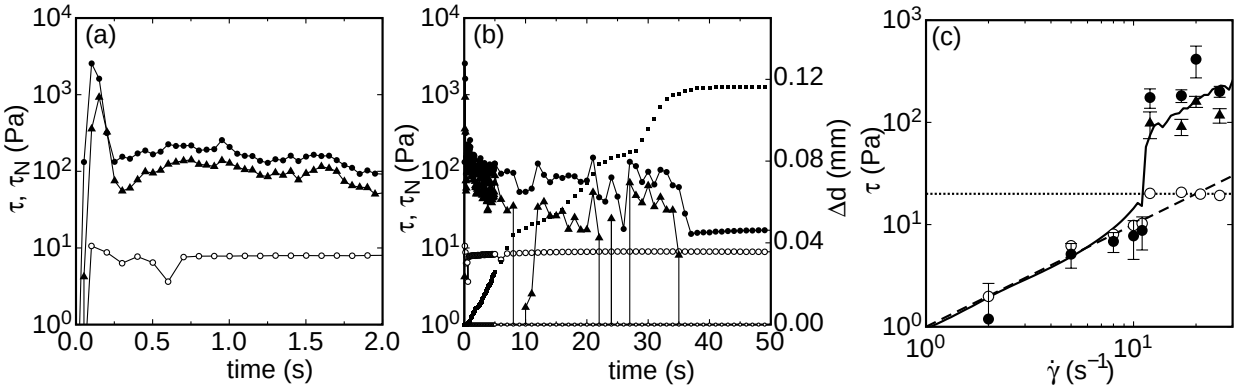


Figure 10: (a) Transient time series of shear stress $\tau$ (circles) and normal stress $\tau_N$ (triangles) in normal force control measurements for cornstarch in water at $\phi = 0.55 < \phi_c$. The sample starts at rest then the shear is switched on at time $t = 0$. Solid symbols: shear rate $\dot{\gamma} = 26$ s$^{-1}$ (above $\dot{\gamma}_c$). Open symbols: $\dot{\gamma} = 8$ s$^{-1}$ (below $\dot{\gamma}_c$). (b) Same data as panel a, but extended to longer times to see the steady state behavior. Right axis: change in gap size $\Delta d$ (small squares). (c) Effective viscosity curves obtained from transient measurements. Solid circles: transient shear stress averaged between 0.4 and 1.0 s after shear starts. Solid triangles: transient normal stress averaged over the same time. Open circles: steady state shear stress at the end of the time series where $\tau_N$ was below the resolution limit for each shear rate. Discontinuous Shear Thickening is suppressed when the normal stress at the boundary is removed. Solid line: stress as a function of shear rate obtained from a steady state viscosity curve for the same sample with fixed gap size. Dashed line: Newtonian scaling.

relative to the static value before each measurement to optimize resolution of the relative normal force. The fact that these three data sets under different measurement conditions collapse onto the same curve suggests a global constitutive relation independent of boundary conditions. Since $\tau/\tau_N$ is near unity and constant over five decades of Reynolds number, this suggests that the measured stresses are compressional in nature, rather than viscous in which case stresses should scale linearly with shear rate or $Re$. This compressive scaling can account for the constant stress term $\tau_c$ in the constitutive relation of Eq. 3, since it is independent of local shear rate and height, but instead is dependent on the normal stress. Such a compressional scaling could be the result of frictional forces or possibly high-inertia flows, although the dominance of gravity in the shear profile shown in Sec. 6, as well as the relative weakness of inertia as explained in Sec. 4, suggest the frictional explanation is more likely. A frictional scaling implies that stresses are redirected in different directions through the bulk of the suspension, a common feature of granular materials in which forces are transmitted along chains of hard particles via frictional contact (Jaeger et al., 1996). Additionally, it implies that positive pressures can be maintained on the system even without solid boundaries on all sides – the role of surface tension in providing a confining stress will be investigated in Secs. 8 and 9.

## 7.2 Transient normal force control measurements

We showed that for steady state measurements with very different boundary conditions the shear and normal stresses always had a fixed ratio near 1, thus the boundary condition determined whether or not shear thickening was observed. Here we show that it applies even to transient measurements as the normal force boundary condition changes, and that shear thickening can be eliminated if the normal force is removed from the boundary as suggested by Fall et al. (2008). To emphasize the generality of these results, we show this result for a different suspension, cornstarch in water, and point out that both this and the results of the previous section are found for both suspensions.

We performed normal force controlled experiments modeled after those of Fall et al. (2008). These measurements were done in the standard parallel plate setup in a normal force controlled mode. The normal force set point is zero relative to the rest state, with an initial gap of $d = 1.08$ mm. The gap size is free to vary during the measurements to adjust the normal force back to the setpoint via a feedback loop. Initially the sample of cornstarch in water at $\phi = 0.55 < \phi_c$ was at rest, then at time $t = 0$ the shear rate was turned on and remained constant for the rest of the experiment. Examples of transient time series of the shear stress and normal stress are plotted in Fig. 10a for two different shear rates. For shear rates below the onset of shear thickening $\dot{\gamma}_c \approx 11$ s$^{-1}$, the stress quickly came to near the steady state value within a fraction of a second and remained there. For shear rates above $\dot{\gamma}_c$, the shear and normal stresses had a large peak initially, exceeding the steady state value by more than an order of magnitude.

Even though the normal force set point was zero, the normal stress can be non-zero in the transient behavior as the gap adjusts via a feedback loop. Longer time series are shown in Fig. 10b along with the variation in gap size. Below $\dot{\gamma}_c$ the normal force did not exceed the threshold to cause the gap to move. In contrast, above $\dot{\gamma}_c$ the gap increased initially due to the transient normal force. The shear stress tracked the normal stress quite well throughout the entire transient process, and they were similar in magnitude. The stresses each decreased as the gap increased, and the gap stopped increasing when the normal stress dropped below the feedback threshold of 20 Pa. Beyond this point the stresses and gap size remained constant, which was measured for at least 200 s in each experiment to confirm that the system was in a steady state.

We summarize the normal force control experiments with effective viscosity curves in Fig. 10c. We show the transient shear and normal stresses averaged between 0.4 and 1 s after the shear was started as solid symbols. Because the response time of these samples to dramatic changes is typically a fraction of a second, while the normal force control feedback loop has a longer timescale, these transient results effectively correspond to a fixed gap boundary condition. They show the same qualitative shear thickening as steady state behavior for fixed gap measurements, indicated by the solid line. Differences between the solid circles and solid line beyond the measurement resolution indicate a difference between steady state and transient measurements. Stress values taken from the end of the test, where $\tau_N = 0$ ($\pm 20$ Pa) and the system was in a steady state, are shown as open circles in Fig. 10c. The effective viscosity curve based on this data is consistent with a Newtonian scaling at shear rates below $\dot{\gamma}_c$. Above $\dot{\gamma}_c$, the shear stress values match up with the normal stress feedback threshold. This can be understood since a normal stress of that magnitude is not enough to trigger the normal force control feedback loop but can still couple to the shear stress. The strong shear thickening in the fixed gap and transient data is totally absent from the $\tau_N = 0$ data. We note that there is no significant dependence of viscosity curves on gap size in this range (Brown et al., 2010b), so the difference must be due to the fact that the normal force is fixed to be zero. This shows that a positive normal stress of comparable magnitude is required to achieve the shear stress associated with shear thickening. In the absence of this confining stress, shear thickening cannot occur, as was suggested by Fall et al. (2008). Without making any assumption about the mechanism for coupling between the normal and shear stresses at values below the normal stress feedback threshold, the open circles in Fig. 10c put an upper bound on the viscous and other non-compressive contributions to suspension viscosity and show that they are not responsible for Discontinuous Shear Thickening.

We have noted that the normal and shear stresses track each other quite well in normal-force-controlled measurements. In fact, in all of the various types of experiments on suspensions that exhibit Discontinuous Shear Thickening in which normal stresses and shear stresses were compared they tended to track each other quite well. For example, we attempted measurements with a fixed normal stress $\tau_N = 0$ and fixed shear stress greater than the normal stress feedback threshold. Since the shear stress is the dominant control parameter of the rheometer, the shear stress reached the set value but the measurements never reached a steady state because the normal stress could not drop, causing the gap to increase until the top plate detached from the sample. Similarly, in experiments by Lootens et al. that measured stress fluctuations in the steady state (Lootens et al., 2005), fluctuations of the normal stress and shear stress were found to be strongly coupled according to a solid frictional relation. This helps explain an earlier result in which an apparent viscosity curve no longer showed shear thickening when positive fluctuations in the shear stress in the steady state were removed from the data (Lootens et al., 2003). Since the shear stress fluctuations were associated with the normal stress, this was in essence showing an effective viscosity curve with no normal stress. Another example comes from our measurements of finite-size effects at very small gap sizes (Brown et al., 2010b), in which the normal stress scaled with and was close in magnitude to the shear stress as it varied with gap size.

# 8 Visible boundary condition

The previous section showed that the sample's boundary conditions are an important factor in whether Discontinuous Shear Thickening is observed. In this section we analyze images of the suspension surface in contact with air to identify the boundary conditions and how they cause the increase in normal stress in the shear thickening regime so we can formulate a model for Discontinuous Shear Thickening in Sec. 9.

## 8.1 Boundary at rest

We first show images of the surface of suspensions at rest. This will provide a baseline for understanding the connection between boundary condition and stresses. The samples consisted of 135 $\mu$m polyethylene spheres density matched in silicone oil, which are opaque and do not settle. These suspensions were placed in a $H = 1.3$ mm deep layer and viewed from the top with direct lighting as shown in Fig. 11. The series of images was taken by starting at a high packing fraction well above the jamming transition ($\phi_c$), then adding oil to reduce the packing fraction for each successive image. At each packing fraction the sample was vibrated at 40kHz with a sonicator for 1 min,

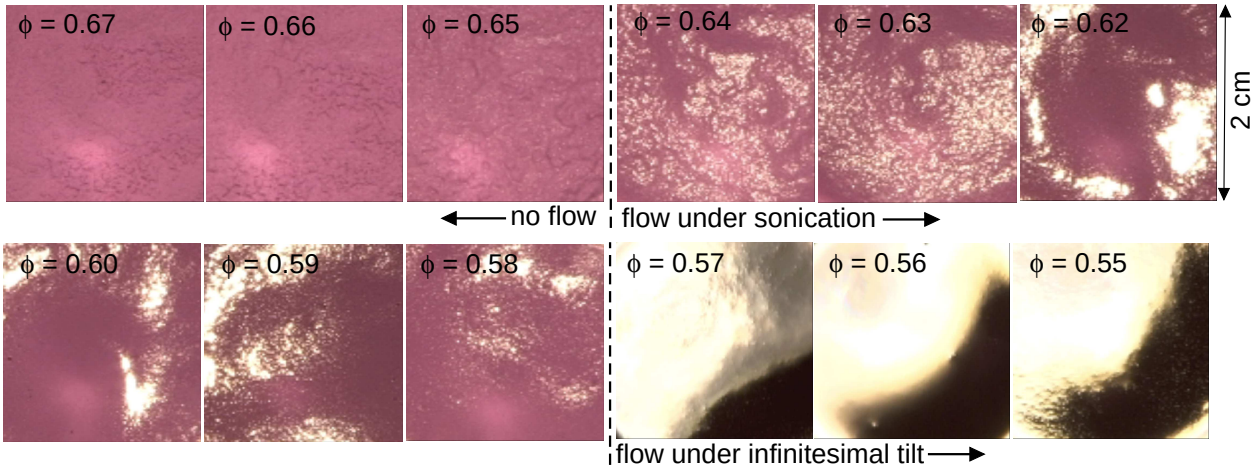


Figure 11: Top views of a static layer of 135 $\mu$m polyethylene spheres density matched in silicone oil. The layer was 1.3 mm deep and each image is 2 cm on a side. Images were taken for different packing fractions given in the corner of each panel. Lighting was direct to emphasize changes in reflectivity. Packing fractions $\phi > 0.64$ did not flow under any amount of tilt. Packing fractions $0.64 \geq \phi > 0.58$ flow while being sonicated, but after stopping sonication, these suspensions no longer flowed at small tilt angles. Packing fractions $\phi \leq 0.57$ flow under even small tilt ($\sim 1$ degree). The reflectance of the surface increased so much when $\phi$ was decreased to 0.57 that the camera became oversaturated by the direct reflection of the light.

tilted during and after sonication to observe whether or not shear occurred, then allowed to rest before the image was taken.

For the highest packing fractions $\phi > 0.64$, the suspension surfaces appear dry and rough and did not flow under tilt during or after sonication. For $0.64 \geq \phi > 0.57$ they appear wetter but still rough. In this range the samples did flow while being sonicated, but afterwards did not flow at infinitesimal tilt angles (measured at $\sim 1^\circ$). However, for several of the packing fractions in this range there was a critical tilt angle $\Theta$ above which flow could be found. For $\phi \leq 0.57$, the samples appeared very shiny and smooth, and they flowed even at infinitesimal tilt angles.

We can connect the value of the critical tilt angle $\Theta$ for flow to the yield stress of the suspension. For a tilt angle $\Theta$, the stress applied by gravity parallel to the surface is $\rho g H \sin\Theta$, which is shown in Fig. 12 for packing fractions in which one was measured. We compare this to the yield stress $\tau_y$ obtained from rheometer measurements in the zero shear rate limit. For $\phi < 0.58$, we measured no yield stress, within our experimental resolution of $10^{-3}$ Pa. There is an absolute uncertainty of about 0.005 in the packing fraction measurements for the yield stress due to the process of loading the sample. Within this uncertainty, the shear stress provided by gravity at the onset of shear under tilt matched with the measured yield stress in the rheometer. This confirms that the visible changes in the surface correspond to changes in the yield stress.

The above analysis implies the roughness of the surface of a suspension can be used as an indicator of the yield stress. At each packing fraction shown in Fig. 11 for $\phi > 0.57$, the sample surface has roughness on a macroscopic scale, i.e. much larger than individual particles. If an asperity of height $H$ forms on the upper surface of a fluid it can remain stable if the yield stress exceeds a value on the scale of $\rho g H$. Thus the maximum asperity size seen on the surface of a suspension can be used to estimate the magnitude of the yield stress of a suspension. For these samples we observed asperities on the order of 1 mm at the highest packing fractions, consistent with the measured yield stresses on the order of 10 Pa and the value $H$ used in the gravitational stress scale.

Here we explain why the roughness of the surface indicates a stress. Similar changes in surface roughness have been observed in jammed suspensions (Cates et al., 2005a), and in free-surface flows, becoming more apparent at higher applied stresses and at higher packing fractions (Loimer et al., 2002; Timberlake and Morris, 2005; Singh et al., 2006). It was argued that these deformations required normal stresses in the suspensions to balance forces from surface tension. If a suspension is unjammed there is free space for the particles to rearrange, so any particles on the surface will be pushed by surface tension to the interior (assuming the liquid wets the particles, which is also a requirement to observe shear thickening (Brown et al., 2010a)), resulting in a flat and shiny surface. In a jammed system, hard particle contacts or other forces counter the force of surface tension, which is transmitted through the system along solid contacts to keep the system in mechanical equilibrium, so the surface remains rough on the particle scale.

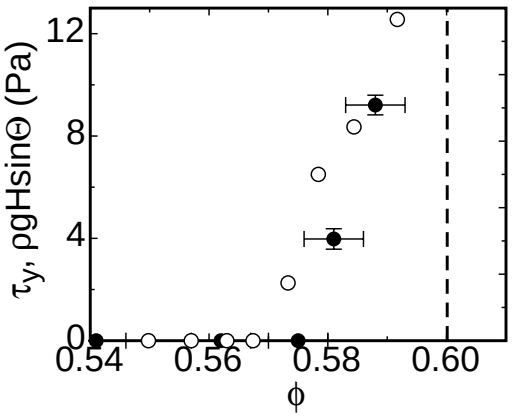


Figure 12: Open symbols: gravitational stress $\rho g H \sin\Theta$ required to initiate shear under tilt for the suspensions shown in Fig. 11. The minimum tilt angle $\Theta$ required for shear is measured relative to a horizontal surface. Dashed line: threshold packing fraction above which the sample did not flow at any tilt angle (without sonication). Solid symbols: yield stress $\tau_y$ obtained from viscosity curves in the rheometer. The jamming transition at $\phi = 0.57$ above which there is a yield stress coincides with the visible change in the surface shown in Fig. 11.

If the particles are between about 1 and 100 $\mu$m, then the grains are large enough to scatter light diffusively and small enough that they cannot be seen individually, so the surface appears rough by eye. This explains why a simple indicator of whether or not a suspension is jammed is whether the surface appears rough or smooth. This easily visible indicator of jamming contrasts with the case of dry grains, where there is no such visual test. The insterstitial liquid allows this sensitive measurement by eye because changes in the fluid level at the surface due to changes in packing density only have to be on the scale of a particle size to dramatically change the surface appearance. We note that for colloidal particles smaller than around 1 $\mu$m, the roughness of the surface becomes smaller than the wavelength of light and no longer scatters diffusively, so the surface of a colloid may even appear shiny if the surface is deformed by particles. This is confirmed by an observation of stable asperities in a jammed colloid of 1.6 $\mu m$ diameter particles – indicating stresses from surface tension – in which the surface remained shiny (Koos and Willenbacher, 2011).

The critical packing fractions for the transitions in Fig. 11 match up with those usually found for the jamming transition (Liu and Nagel, 1998). The transition at $\phi = 0.64$ corresponds to random close packing for frictionless spheres, above which packings of are jammed and below which they can flow (O'Hern et al., 2003). When comparing to other published values for critical packing fractions, It is reasonable to expect an absolute uncertainty in the range of 0.01 in the packing fraction due to factors such as a finite size effect and polydispersity in the particle sizes, and sample preparation. Experimentally it is usually found that packings of spheres remain mechanically stable, i.e. have a yield stress down to packing fractions around 0.56-0.60 depending on density difference $\Delta\rho$, called random loose packing (Onoda and Liniger, 1990; Jerkins et al., 2008). Packing fractions closer to $\phi = 0.64$ can only be reached if the packings are vibrated which mobilizes the particle contacts, effectively eliminating the effect of friction (Knight et al., 1995). This explains why in the range $0.64 \geq \phi > 0.57$ our suspensions flow under sonication but are otherwise jammed.

We note the visible transition at $\phi = 0.64$ in Fig. 11 is not always observed, depending on sample preparation. If we do not sonicate, the samples can appear to be dry until they are diluted all the way down to $\phi = 0.57$. This could be because without the mobilization of particle contacts allowed by sonication, the suspension may not be able to pack more densely than $\phi = 0.57$, perhaps trapping air bubbles, or to make up the extra space the liquid may retreat to the interior of the sample. Despite this hysteresis effect in the visible transition at $\phi = 0.64$ during preparation, rheology measurements with preshear consistently show the onset of a yield stress at the same packing fraction.

## 8.2 Dilation

We just demonstrated that a visible change in the surface of a suspension can correspond to a qualitative change in the global rheology where surface roughness indicates stresses from surface tension are transmitted through the suspension. In systems that show Discontinuous Shear Thickening, it has been long known that there can be a visible change in the surface of suspensions at the onset of shear thickening (Metzner and Whitlock, 1958; O'Brien and

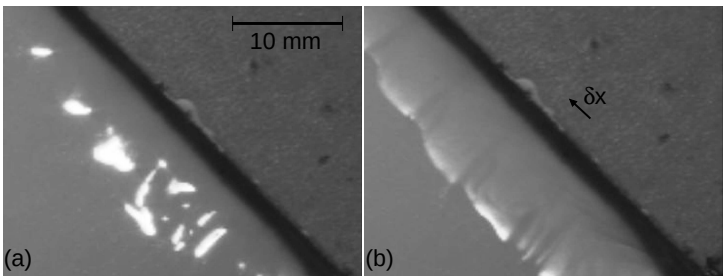


Figure 13: Top views of a 2.4 mm deep layer of cornstarch in water. (a): Below $\phi_c$ in a shear cell at rest. (a) at a shear rate above $\dot{\gamma}_c$, taken after a shear displacement of $\delta x = 2.5$ mm relative to panel a. Dilation can be observed as an increase in surface roughness in the sheared region near the wall.

Mackay, 2000; Smith et al., 2010). It was understood early on that this was due to dilation (Metzner and Whitlock, 1958). When granular packings dilate under shear, they take up more space than at rest, and consequently the liquid is then sucked away from the boundary into the enlarged gaps between grains, so the surface appears rough by eye.

This visible effect of dilation is shown for a suspension of cornstarch (14 $\mu$m) in water below $\phi_c$ in Fig. 13. The suspension was in a 2.4 mm deep layer and viewed from above. One of the side walls could be displaced to shear the suspension. Before shear the surface of the suspension looked wet and shiny, as seen in panel a. When the upper right wall was sheared at a rate exceeding the onset of shear thickening the nearby suspension appeared rough, shown in panel b. As soon as the shear rate dropped, the surface appeared smooth and shiny again. This behavior is shown in supplementary video 3. We observed that the onset of visible dilatancy corresponds closely to the onset of shear thickening, consistent with previous observations that the shear thickening corresponds to the onset of dilation (Metzner and Whitlock, 1958; Smith et al., 2010).

Usually we find suspensions will show Discontinuous Shear Thickening in rheological measurements if the surface changes from shiny to rough when sheared, indicating dilation. At low packing fractions, the surface remains smooth under shear because the packing fraction is too low for granular dilation to affect the surface, since volume changes from dilation are typically only a few percent (Reynolds, 1885; Onoda and Liniger, 1990). Alternatively, if the suspension has a yield stress, the surface may be always rough and not change with shear rate, even if the packing still dilates with shear. Thus, the conditions where a change in the surface from dilation is observed seem to correspond to the conditions for suspensions to show Discontinuous Shear Thickening.

There is a notable exception to the rule that a visible change in the surface from dilation indicates shear thickening. Settling particles in a Couette cell were seen to dilate but did not shear thicken, and instead a yield stress was measured (Metzner and Whitlock, 1958; Fall et al., 2009). However, a simple argument can explain this behavior. The weight of the particles in a vertical column of height $H$ pushes on the side walls which are supposed to shear, resulting in a yield stress on the scale of $\Delta\rho g H$ which can be on the order of kPa (Fall et al., 2009), well above the shear thickening stress regime which we observed for glass spheres from 10-100 $\mu$m in a parallel plate geometry which does not have this yield stress (see Fig. 17). In the case of vertical walls, the side of the suspension is still jammed at rest which prevents shear thickening, but the top is not, so the suspension falsely appears unjammed when viewed from the top. A more general conclusion is that dilation is necessary for Discontinuous Shear Thickening but not sufficient because shear thinning stresses must be small compared to shear thickening stresses or else the shear thickening will be hidden (Brown et al., 2010a).

Now that we have established the connection between boundary conditions and stresses, we want to directly address what the boundary looks like on the particle scale. To this end we use a sample of opaque 150 $\mu$m diameter $ZrO_2$ particles in mineral oil at $\phi = 0.54$ in a standard parallel plate rheometer setup with a gap size of 890 $\mu$m. A video camera was focused at a point on the surface of the suspension with the line of sight tangent to the surface to best view any radial variations in the boundary position due to dilation. The sample is shown at rest in Fig. 14a, in which case it had a smooth surface. The same sample is shown in panel b at a steady shear rate of 3 $s^{-1}$, corresponding to $\tau_{max}$ at the upper bound of the shear thickening regime. The boundary appears bumpy as particles penetrate the liquid-air interface. The dynamic behavior is shown in supplementary video 4. The penetration of the liquid-air interface by the particles can also be seen in the shear profile videos of $ZrO_2$ as texture differences indicating contact lines on particle surfaces in supplementary videos 1 and 2. By reference to the edge of the rheometer plate (red line), it can be seen that the sample has expanded radially relative to the rest state by about 50 $\mu$m, corresponding to $0.3a$ or a volume increase of 0.8%.

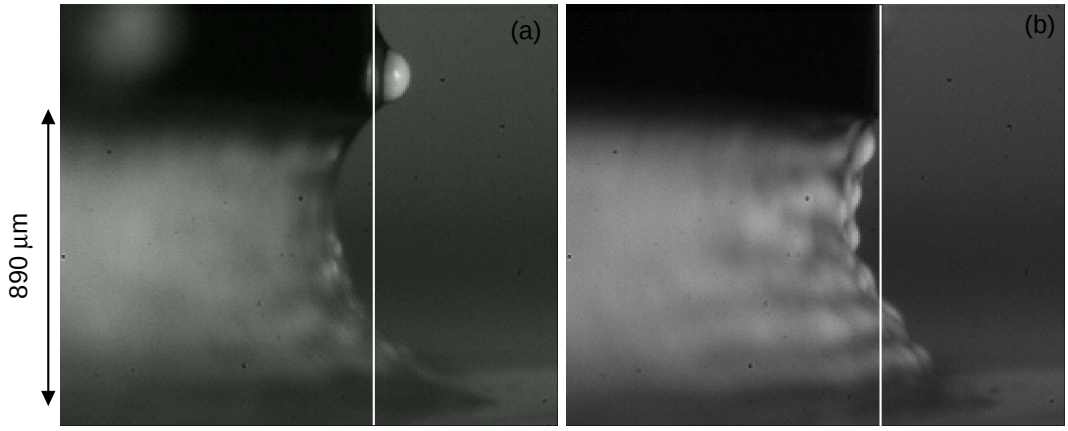


Figure 14: Images a suspension of 150 $\mu$m $ZrO_2$ particles in mineral oil in the standard parallel plate setup with a gap of 890 $\mu$m. The camera is focused at a point on the edge of the suspension, with the line of sight tangent to the surface to view radial variations in the boundary position. The rest of the image is out of focus because of the large amount of depth in the image. (a) The suspension at rest. (b) The suspension is sheared at constant shear rate of 3 Hz corresponding to $\tau_{max}$. It can be seen that shear results in both dilation of the suspension and increased local curvature at the surface. Vertical lines: reference lines indicating the plate edge in each image.

# 9 Capillary forces

In the previous section showed that when a dense suspension dilates under shear, the particles penetrate the liquid-air interface. The curvature of the liquid-air interface caused by this can produce stresses from surface tension. Indeed, it has been suggested that capillary forces at boundaries could play an important role in the rheology of shear thickening suspensions (Holmes et al., 2003, 2005; Cates et al., 2005b). To understand the consequences of surface tension at the boundary, in the following we propose a mechanism leading to an increased shear stress. When dilation causes particles to penetrate the edge of the suspension to create a curved liquid-air interface, the scale of the radius of curvature $r$ of the liquid-air interface with surface tension $\gamma$ becomes comparable to the particle size $a$ (Loimer et al., 2002). This produces a stress from surface tension pushing the particles towards the interior of the suspension. We estimate this stress from surface tension to be on the scale of $\gamma/r \sim \gamma/a \sim 100$ Pa for 100 $\mu$m particles, a significant stress in the context of the rheological measurements. If the particles were not tightly packed, they would be pushed to the interior of the sample by this stress. However, the fact that the particles continue to penetrate the surface in the steady state implies that, in the absence of inertial effects, forces must be transmitted all the way through the packing. This could be achieved either through an effective granular temperature, or force chains between frictional contacts which may be dynamically changing in the case of dilation under shear. The dominance of gravity over kinetic energy in the shear profile shown in Sec. 6 suggests the frictional contacts are more likely. In either case, the stress from surface tension can then be considered a confining stress on the packing which is transmitted throughout the suspension by these force chains. In a granular packing, forces tend to be redirected easily as contacts between particles can occur at a variety of angles, so a confining stress on one side will lead to a similar normal stress being felt on the top and bottom plates. These normal stresses between particles result in shear stresses by frictional contacts with the rheometer plates, as was seen in Figs. 9 and 10, leading to the increased dissipation corresponding to Discontinuous Shear Thickening. In the remainder of this section we quantitatively connect the measured shear stresses to the confining stress scale from surface tension $\gamma/a$ to test this model.

## 9.1 Relating dilation to confining stress

To quantify the dilation, we measured the mean radial displacement of the surface during shear seen in a tangent view as in Fig. 14. We did this for several different steady state shear rates in a sample of opaque 135$\mu$m polyethylene spheres in silicone oil at $\phi = 0.56$. For each measurement, we started the sample at rest, then sheared at a constant shear rate until the stress reached a steady state for some time, then stopped the shear to observe the relaxation to rest. We repeated the cycle of shear followed by resting a total of 5 times. The edge of the sample was tracked throughout these measurements. The dilation $\delta$ was measured as the mean radial displacement of the edge between the steady state shear and rest states, averaging over the height of the sample and over at a period of at least 10

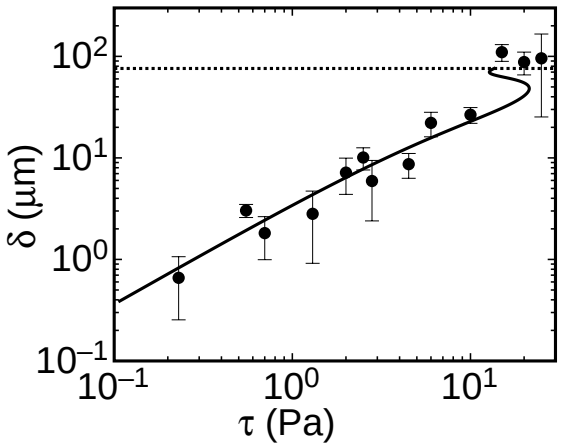


Figure 15: The radial dilation $\delta$ measured as a function of shear stress for 135 $\mu$m polyethylene spheres in silicone oil. Solid line: relationship between $\delta$ and $\tau$ for a model in which there is a confining stress from surface tension $\tau \propto \gamma/r(\delta)$ where the local radius of curvature $r(\delta)$ is determined geometrically. A proportionality coefficient of 0.14 shifting the curve horizontally is used to fit the data. Dashed line: dilation value where the contact line is expected to reach the 2nd layer of particles resulting in a dramatic increase in confining stress with dilation.

s and a strain of at least 2 in the steady state for each experiment. The measured dilation is plotted versus the corresponding steady state stress values in Fig. 15. Plotted error bars correspond to the standard deviation of $\delta$ measured over the 5 cycles. All points shown correspond to stresses above $\tau_{min}$. At lower stresses we could not resolve any dilation below our resolution limit of 0.5 $\mu$m. The upper end of the shear thickening regime corresponds to $\tau_{max} = 2$ Pa for this sample.

We can calculate a typical radius of curvature of the liquid-air interface as it contracts for a given particle dilation $\delta$, given the contact angle and conservation of volume. This allows us to estimate a confining stress scale from surface tension $\gamma/r(\delta)$. Details of this calculation are shown in the appendix. Briefly, the initial state with a relatively large radius of curvature corresponds to $\delta = 0$. As $\delta$ increases, the surface becomes more curved and the radius of curvature decreases, with the scale of the radius of curvature set by the particle size when the dilation is around a particle radius. This model prediction is shown in Fig. 15 where $\delta$ is plotted vs. the predicted stress scale $\gamma/r(\delta)$. A free parameter for the scale factor of 0.14 on the stress scale is used to fit the data. The qualitative agreement in the model slope with the data in Fig. 15 confirms that the confining stress scaling as $\gamma/r$ is a good estimate for the measured shear stress. The fit coefficient within an order of magnitude of 1 confirms that the amount of dilation is on the right scale to provide the measured stress.

The dotted line in Fig. 15 corresponds to the dilation value where the contact line is expected to reach the 2nd layer of particles from the surface (see appendix for calculation). At this point the confining stress should increase rapidly as more contacts are made with small curvature. Because the calculation of confining stress from dilation is not monotonic around this region, the dilation is not single-valued function of confining stress. The lower portion of the curve is expected to be unstable since more dilation would provide less of the stress required to confine the suspension to a smaller volume. The agreement of the dilation measurements with the dotted line beyond the point where the calculation becomes multi-valued supports this interpretation.

As the dilation increases and the contact line recedes further into the interior, a lower limit for the value for the curvature must be reached as it is limited by the interstitial gap size. The corresponding limiting confining pressure has been measured in an analogous system in which a fluid interface was driven through a porous medium, in which case the required driving pressure went to $0.7\gamma/a$ in the limit of zero flow rate (Weitz et al., 1987). This confining stress sets the scale for the upper bound on the component of the shear stress due to capillary forces on the order of $\gamma/a$ in the limit of large $\delta$. The value of $\tau_{max} = 2$ Pa corresponding to the data in Fig. 15 is significantly below the limiting confining stress regime, suggesting that dilation by a fraction of a particle width was enough to obtain a fully developed shear flow and the limiting confining stress is not necessarily reached in the shear thickening regime.

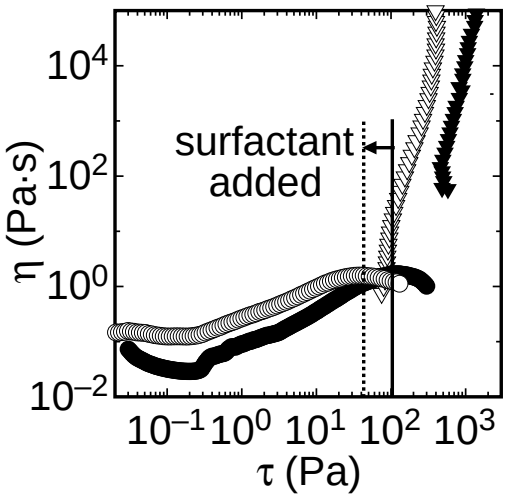


Figure 16: Viscosity curves for 100 $\mu$m glass spheres in liquids with different values of surface tension. Solid symbols: particles were suspended in water. Open symbols: particles were suspended in water with surfactant (above the critical micelle concentration). Triangles: $\phi = 0.58 > \phi_c$. Circles: $\phi = 0.56 < \phi_c$. Solid line: $\tau_{max}$ without surfactant. Dotted line: $\tau_{max}$ with surfactant. Both $\tau_{max}$ and the yield stress above $\phi_c$ decreased when the surface tension was reduced.

## 9.2 Surface tension scaling

To confirm the role of capillary forces, we performed a set of rheological measurements in which we varied the surface tension of the liquid-air interface. To vary this surface tension, we added surfactant to 100 $\mu$m glass spheres in water. The surfactant used was Palmolive dish detergent, which was first mixed in water above the critical micelle concentration which reduces the surface tension with air by about a factor of 3 compared to pure water and air. Viscosity curves are shown with and without surfactant and at different packing fractions in Fig. 16. We first compare the viscosity curves for jammed suspensions at $\phi = 0.59 > \phi_c$. These viscosity curves correspond to yield stress fluids. The value of the yield stress is reduced by a factor of 2.4 with the addition of the surfactant, about the same as the surface tension was reduced.

We next compare the viscosity curves at $\phi = 0.56 < \phi_c$ in Fig. 16. The vertical shift in the viscosity at low shear rates can be attributed to the increase in the zero shear viscosity with the addition of the surfactant. In terms of stress scales, there is a decrease in $\tau_{max}$ by a factor of 2.4 when the surfactant is added, and no resolvable change in $\tau_{min}$. The reduction in both $\tau_{max}$ and the yield stress $\tau_y$ above $\phi_c$ is comparable to the reduction in surface tension with the addition of surfactant, again consistent with a model in which these stresses scale with surface tension.

We note that in principle the addition of surfactant can change other relevant parameters. The stress from surface tension on a boundary typically scales as $(\gamma/r)\cos\theta$ where $r$ is the radius of curvature and $\theta$ is the contact angle, where both $\gamma$ and $\theta$ can vary with the addition of surfactant. The addition of a surfactant can reduce $\theta$, increasing the stress from surface tension. However, we start with a liquid that wets glass pretty well, as this is a requirement to observe shear thickening (Brown et al., 2010a), so $\cos\theta \approx 1$ even before the addition of surfactant. The addition of surfactant can also affect the value of $\tau_{min}$ in cases where the particle-liquid surface tension is dominant (Brown et al., 2010a), but for these 100 $\mu$m glass spheres in a wetting liquid the dominant force affecting the onset is gravity (Fig. 5).

The results in Fig. 16 suggested that the upper stress scales $\tau_{max}$ and $\tau_j$ (the scale of the yield stress for $\phi > \phi_c$) scale with the surface tension at the liquid-air interface. To more generally test the predicted stress scale $\tau_{max} \sim \gamma/a$ including the particle size scaling, we plot measured values of $\tau_{max}$ vs. $\gamma/a$ for the wide range of Discontinuous Shear Thickening suspensions we have studied in Fig. 17. Each point corresponds to a different suspension, with a wide range of different particle materials, shapes and sizes, and different liquids, and was obtained by averaging $\tau_{max}$ from viscosity curves at several packing fractions. We also included data from other papers in cases where $\tau_{max}$ was measured. It is seen that for this wide variety of suspensions, covering four orders of magnitude, $\tau_{max}$ falls in a band that scales as $\gamma/a$. We note that for each Discontinuous Shear Thickening suspension we studied, the two stress scales $\tau_{max}$ and $\tau_j$ are always within an order-of-magnitude of each other, as was seen, for example, in Fig. 16 and Brown and Jaeger (2009), suggesting that $\tau_j$ also scales with $\gamma/a$. In many measurements of colloids, the upper

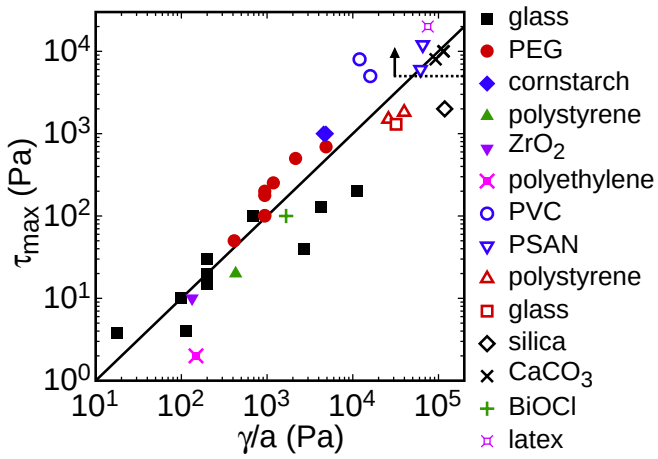


Figure 17: The stress at the upper bound of the shear thickening regime $\tau_{max}$ for a variety of suspensions plotted against the confining stress scale from surface tension $\gamma/a$. Particle materials are listed in the key. Solid symbols: measured by us. Open symbols: polyvinyl chloride [PVC, circles (Hoffman, 1972)], polystyrene-acrylonite [PSAN, down-pointing triangles (Hoffman, 1972)], polystyrene [up-pointing triangles (Boersma et al., 1991)], glass [square (Boersma et al., 1990)], silica [diamond (Bender and Wagner, 1996)], $CaCO_3$ [diagonal crosses (Egres and Wagner, 2005)], BiOCl [cross (Bertrand et al., 2002)], latex [crossed circle (Laun et al., 1991)]. The solid line corresponds to a scaling $\tau_{max} = 0.1\gamma/a$. Dotted line: lower bound on $\tau_{max}$ for measurements in which $\tau_{max}$ was not reached (Maranzano and Wagner, 2001a), which often occurs in colloid measurements.

end of the shear thickening regime was not reached. If there is an upper bound, it would have to be above the range measured. This is especially a problem with colloids because the expected scale of $\tau_{max}$ for small particles exceeds the measuring range of many rheometers. For example, our Anton Paar MCR 301 rheometer has an upper limit of 3800 Pa for the Couette cell or 65,000 Pa for the 25 mm diameter parallel plate. This lower bound on $\tau_{max}$ based on the limited measuring range is illustrated as the dotted line in Fig. 16, using data from Maranzano and Wagner (2001a) as an example.

There is variation in the value of $\tau_{max}$ in the band shown in Fig. 17 by about an order of magnitude. There are many factors that could contribute to the precise value of the confining stress and the resulting shear stress. For example, the normal stresses do not have to be exactly the same on each surface as would be the case for a pressure acting on a fluid. Instead the stresses are related by a coefficient of order 1 (Janssen, 1895; Sperl, 2006). Since the confining stress can put a normal stress on the top plate via chains of particle contacts, then a component of the shear stress comes from friction, related to the normal stress by an effective coefficient of friction as seen in Fig. 9. The contact angle $\theta$ has been left out of the force equation since it is not known in many cases. The dependence of dilation on the shear rate must also play a significant role, as seen in Fig. 15. Geometric factors including particle shape and roughness also should play a role that has not yet been studied. Considering all of these dimensionless factors of order 1 that can affect the shear stress which are not all known or easily measured, we will not go beyond using the order-of-magnitude stress scale of $\gamma/a$ as an estimate for $\tau_{max}$.

We now address why surface tension determines $\tau_{max}$ and $\tau_j$ rather than $\tau_{min}$. We already argued that the confining stress from surface tension produces normal stresses between particles and the walls that results in a shear stress via friction. This confining stress increases precipitously in the shear thickening regime as the amount of dilation increases with shear rate. The maximum confining stress from surface tension should be on the order of $\gamma/a$ if $\delta$ reaches the order of $a$ or larger. Beyond the point where the confining stress reaches its maximum, any additional shear stress must come from other sources, which are likely weak compared to the confining stress if shear thickening is observed, so the viscosity should drop off beyond the maximum confining stress. Thus the maximum confining stress should correspond to $\tau_{max}$. Above $\phi_c$ where the suspension is jammed, particles penetrate the surface even without shear as seen in Fig. 11, so the yield stress scale $\tau_j$ should also be set by the confining stress from surface tension.

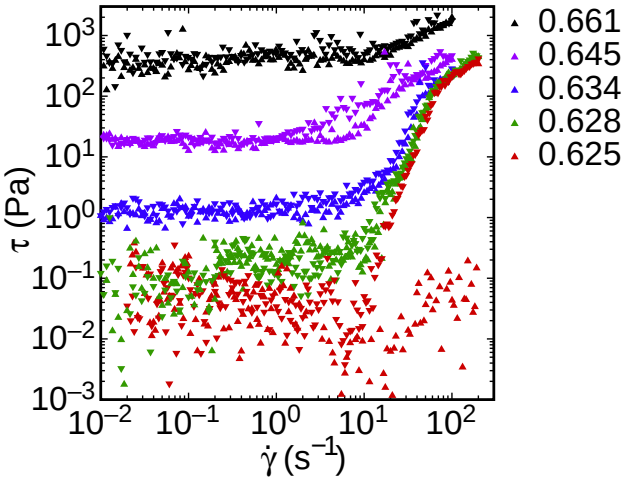


Figure 18: Stress vs. shear rate curves for 500 $\mu$m diameter glass spheres in a solid-walled rhoemeter with *no liquid*. Packing fractions $\phi$ shown in the key; higher curves correspond to larger $\phi$. Discontinuous Shear Thickening is still seen, confirming that viscous interactions are not necessary.

# 10 Solid boundaries

In the previous section we showed that under boundary conditions such that particles penetrate the liquid-air interface, surface tension provides a confining stress which sets the scale of the stress response, specifically $\tau_{max}$ and $\tau_j$. While a liquid-air interface at the boundary is typical for rheometer measurements, closed systems with solid walls are also of interest. In this section we will generalize the role of the confining stress from different sources to understand the rheology of dense suspensions in closed systems.

For measurements in a closed system, we used the parallel plate setup with solid walls shown in Fig. 1b. The hard walls confined large grains within the container volume without the need for the surface tension of the liquid, so we can determine the role of the liquid by comparing measurements with and without liquid. We first show stress/shear-rate curves for shear rate controlled measurements of dry 500 $\mu$m glass spheres in Fig. 18. Without liquid, the packing fraction is determined by the container volume which can be varied with the gap size. Thus, for a series of measurements with a fixed volume of particles, the gap height determines the packing fraction, with smaller gaps corresponding to higher packing fractions. We give relative packing fraction values accurate to 3 decimal places to compare curves in Fig. 18, but absolute uncertainties on packing fractions are still around 0.01.

An important result from Fig. 18 is that the curves show Discontinuous Shear Thickening that is qualitatively similar to measurements of suspensions in standard rheology setups, despite the fact that there is no liquid. Thus, the interstitial liquid or viscous stresses are not a necessary component for shear thickening when the grains are confined by other means.

A large hysteresis loop can be seen for $\phi = 0.625$ in Fig. 18. This is the threshold beyond which – at larger gap sizes, corresponding to lower packing fractions – not only the yield stress but also the measured shear stress was below the resolution limit suggesting contact between the plate and grains was lost. This emphasizes that a key role of the liquid is simply to keep contact with and transmit stress between the particles and the plate.

We repeated these measurements with water as a solvent filling the measurement volume and surrounding so there was no liquid-air interface near any particles. With water, contact between the suspension and plates could be maintained at larger gaps (lower packing fractions). However, no significant difference was seen in the qualitative aspects of Discontinuous Shear Thickening or in the scale of $\tau_{max}$ with or without water.

An upper bound on the jamming transition can be identified by the point where the shear stress drops below the measurement resolution at $\phi = 0.62$. The jamming transition can be at a significantly higher packing fraction dry than with liquid because of the larger density difference between the particles and surrounding fluid (Onoda and Liniger, 1990). With a solid wall, the yield stress did not plateau at high packing fractions like in the case of a liquid-air interface, but rather increased dramatically as the packing fraction was increased as seen in Fig. 18. This continued up to the maximum stress the rheometer can apply. This can be expected if the confining stress comes from the stiffness of either the wall or the particles, in which case the confining stress increases as the solids are further compressed (O'Hern et al., 2003). This is in contrast to the confining stress from surface tension which is limited by a constant scale as packing fraction is increased beyond jamming (Brown and Jaeger, 2009), which is due

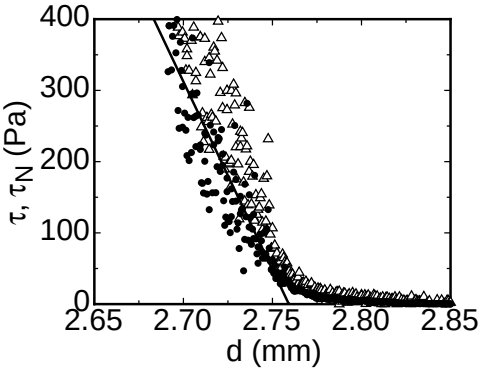


Figure 19: Shear stress $\tau$ and normal stress $\tau_N$ vs. gap size $d$ for a sample of 500 $\mu$m glass spheres with no liquid under compression with solid walls. The sample is compressed at a rate of 0.25$\mu$m/s and sheared at a rate of 1 Hz. The shear stress is close to the zero shear rate limit, so the measured $\tau$ is a good proxy for the yield stress. The solid line is a linear fit used to obtain the per particle stiffness $k$ of the system of sheared grains and solid wall in series.

to the fact that the radius of curvature is limited by the particle size.

To connect $\tau_{max}$ to a confining stress for closed systems, we made measurements of the compressional stiffness of the tool and sample in series. We observed that the rearrangement of particles under shear makes the suspensions much more compliant than under compression alone. Thus we sheared the samples while measuring the compressional stiffness to better match the usual experimental conditions. The sample was slowly compressing at a fixed rate of 0.25 $\mu$m/s while also shearing at a fixed rate of 1 Hz (3 mm/s). The shear rate was much faster than the compression rate so that the packing has time to rearrange as it is being compressed, but slow enough that the shear stress is still near the zero shear rate limit as seen in Fig. 18. The measured shear and normal stresses are shown in Fig. 19. We note that the stiffness under shear is much less than the value obtained by compressing the sandpaper by itself, which is the weakest component of the wall. Thus the presence of the grains has a significant effect on the effective stiffness, despite the fact that the material stiffness is much higher than that of the sandpaper.

In the case with a liquid-air interface, we found the the confining stress to scale as $\delta\gamma/a^2$ (Fig. 15). If for the solid walls, the confining stress also comes from dilation against the boundary, it should provide a restoring stress against dilation from the boundary of $\delta\partial\tau/\partial d$. To obtain an analog for the surface tension we define a stiffness per particle as $k = -a^2\partial\tau/\partial d$ so that the above expressions for confining stress become equal in the case where the per particle stiffness comes from surface tension (i.e. when $k = \gamma$). This is a modification of the usual definition of stiffness for an elastic material, normalized for a wall whose cross-sectional area is $a^2$, near that of a particle. This modification makes this per particle stiffness independent of the surface area of the boundary. We can obtain $k$ from the slope in Fig. 19.

We plot values of $\tau_{max}$ vs. a confining stress scale equal to the boundary stiffness per particle over particle size $k/a$ in Fig. 20 each for the wet and dry 500 $\mu$m glass spheres. We also measured a set of stress/shear-rate curves and compression curves for the wet glass spheres with a layer of soft foam rubber inserted between the top plate and sample as shown in Fig. 1b, and the corresponding values of $\tau_{max}$ and $k/a$ are also plotted in Fig. 20. We also measured a set of data without sandpaper on the plate surfaces, which resulted in a much lower stiffness than with the sandpaper, despite having a harder surface, suggesting significant slip. For comparison to the standard parallel plate measurements with a liquid-air interface, we plot $\tau_{max}$ vs. $\gamma/a$ for one such experiment with the same particles, using the surface tension $\gamma$ as a proxy for the stiffness per particle, which was also plotted in Fig. 17. As a final comparison, we plot $\tau_{max}$ vs. an effective stiffness per particle taken from Fig. 15 as $k = a^2(\partial\delta/\partial\tau)^{-1}$ in the nearly linear regime. All of these experiments are consistent with the relationship $\tau_{max} = 0.05k/a$. This scaling confirms that, for a wide range of boundary conditions including both liquid and solid boundaries, and even when there is a large amount of slip, the scale of $\tau_{max}$ is set by the confining stress which is proportional to the per particle stiffness of the boundary. The similar values obtained when using $k/a$ or $\gamma/a$ as the effective stiffness emphasizes the fact that the per-particle stiffness $k$ generalizes the role of the surface tension with a liquid-air interface to the case with a solid wall. This means that the slopes of Figs. 17 and 20 are related, although with the value of the coefficient relating $\tau_{max}$ and $k/a$ being suspension dependent. The final comparison with the stiffness obtained from the inverse slope of Fig. 15 confirms the role of dilation in pushing against the boundary, and suggests that the confining stress could be written directly as $\tau_{conf} = \delta k/a^2$ for a linear elastic boundary.

Since $k/a$ represents the restoring stress from the boundary for $\delta = a$, and the coupling coefficient between shear

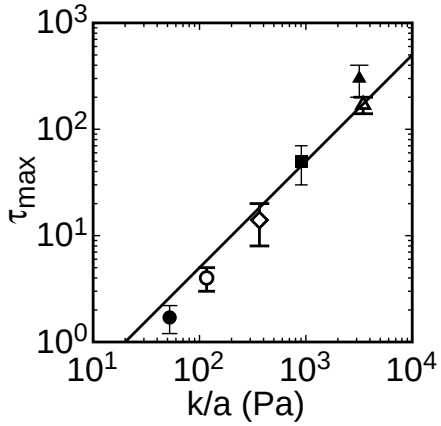


Figure 20: Maximum stress of the shear thickening regime $\tau_{max}$ vs. the confining stress scale $k/a$ due to the restoring force of the boundary with per-particle stiffness $k$. Data are for 500 $\mu$m glass spheres under several different boundary conditions. Solid triangle: hard wall rheometer setup, with particles suspended in water. Open triangle: hard wall, no liquid. Solid square: hard wall with a soft foam rubber insert, with particles suspended in water. Open circle: in a standard parallel plate setup with a liquid-air interface, where we use the surface tension to represent the per particle stiffness (i.e. $k = \gamma$). Solid circle: polyethylene in mineral oil from Fig. 15 where we calculate $k = a^2(\partial\delta/\partial\tau)^{-1}$. The solid line has a slope of 1, corresponding to a stress response proportional to the restoring force of the boundary against a typical dilation of the sample by $\delta \approx 0.05a$.

and normal stresses tends to be close to 1 (Fig. 9), the slope of 0.05 between $\tau_{max}$ and $k/a$ suggests the restoring stress of the boundary is against a dilation of approximately $\delta \approx 0.05a$ at $\tau_{max}$. This is the order of the expected dilation required to allow spherical particles to escape out of the wells they can sit it at the interstices between three neighboring particles. Similarly, dilation on the order of a percent of the sample thickness is typical of measurements of sheared granular packings (Reynolds, 1885; Onoda and Liniger, 1990).

In the experiments with a liquid-air interface, the boundary at the side determined the confining stress, while in the solid wall experiments, the top wall with the soft layer determined the confining stress. In each case, the most compliant boundary determined the confining stress. This is due to the fact that the stiffness of a collection of materials in series is determined by the most compliant material. Whether the most compliant boundary is on the side or the top does not matter, since the frictional relation between shear and normal stresses suggest that the stresses are similar on all of the boundaries (Janssen, 1895).

# 11 Discussion

## 11.1 Dominant stress scales

So far we have described the boundaries of the shear thickening regime $\tau_{min}$ and $\tau_{max}$ in terms of dominant stress scales in different parameter regimes. The dominance of different parameter regimes in a generic sense is not unexpected, as for smaller particles (i.e. colloids), Brownian motion and electrostatic interactions tend to be dominant, while for larger particles (i.e. suspensions) gravity tends to be dominant. Here we discuss the onset stress scalings in the most general terms possible to describe a single mechanism for shear thickening that applies to all of the parameter regimes, and delineate where in phase space each regime is dominant.

First we want to focus on the common feature of the onset scaling laws for $\tau_{min}$. In a previous work we considered the effect of particle attractions from various sources, including particle-liquid surface tension and induced attractions from external fields (Brown et al., 2010a). In each case the attractions resulted in a yield stress. The scale of $\tau_{min}$ was set by the shear stress required to overcome roughly the two-particle attractive force (per cross-sectional area of a particle) to shear them apart. In Sec. 5, we found that in suspensions of particles large enough to settle the scale of $\tau_{min}$ is set by gravity rather than attractions (Fig. 5). The shear stress needs to be enough to exceed the weight of a particle per cross-sectional area to overcome friction. The common criterion for the onset of shear thickening in all of these cases is that the applied shear stress must exceed all local stress barriers that are responsible for holding the particles in place. Once this threshold is exceeded, local shearing between grains can occur, which leads to dilation

and increased confining stresses resulting in shear thickening.

In cases where interparticle attractions are dominant they also tend to set the scale of the yield stress (Brown et al., 2010a). Just above the yield stress, the confining stress can start to grow as shear causes dilation, but there must be at least a small shear thinning regime before the confining stress becomes dominant and shear thickening is seen (Gopalikrishnan and Zukoski, 2004; Brown et al., 2010a). Indeed, Metzner and Whitlock (1958) found the onset of dilatancy at slightly lower shear rates than the onset of shear thickening. In other words, the onset of shear thickening corresponds to a transition in the dominance of different stress and not necessarily where the mechanism for shear thickening first appears.

With this picture we can now try to understand the case of colloids in which the particles have a repulsive electrostatic potential. While attractive particles may have to be pulled apart to shear, repulsive particles may have to be pushed around each other to shear. If the particles push against each other they end up pushing against all of the confining stresses, whose net response is still determined by the softest component of the system. This means we expect the onset stress to be set by the scale of the two-particle interaction stress scale regardless of whether it is attractive or repulsive. Maranzano and Wagner (2001a) measured $\tau_{min}$ for repulsive (charge-stabilized) colloidal particles from 80 to 700 nm in diameter and known zeta potentials $\zeta$. A power law fit to their measurements for the onset of shear thickening gave $\tau_{min} \propto a^{-2.11\pm0.16}$. An electrostatic calculation of the two-particle repulsive force over the cross-sectional area of spherical particles gives a stress scale of $16\epsilon\zeta^2/a^2$ for a liquid permittivity $\epsilon$. This has both the same scaling and magnitude within about a factor of 2 of their data, consistent with the idea that the onset of shear thickening is set by the repulsive stress scale. The same scaling was argued for by Hoffman (1998). This onset scaling is consistent with the general criterion that the applied shear stress must exceed the local stress barrier that is responsible for holding particles in place. The idea that it does not matter whether the interparticle potential is attractive or repulsive is familiar in jammed systems. In simulations of confined repulsive particles it has been shown that the shape of the potential is not relevant to whether the system will jam, but the magnitude of the potential does set the scale of the stress moduli in either case (O'Hern et al., 2003). On the other hand, if the particles have weak attractions in addition to hard-core repulsions, yield stresses have been measured on the scale of the attractions (Trappe et al., 2001).

The regime that has received the most attention theoretically is the Brownian-motion dominated regime. In this regime the onset of shear thickening has been found to correspond to a critical Peclet number $Pe_c = 6\pi\eta\dot{\gamma}a^3/kT = 100$ (Farr et al., 1997), or equivalently an onset stress $\tau_{min} = 50kT/3\pi a^3$ (Maranzano and Wagner, 2001b; Gopalikrishnan and Zukoski, 2004). This scale is the osmotic pressure, which is an effective repulsive stress. It is notable that this Peclet number scaling for the onset works both for Discontinuous and Continuous Shear Thickening (Maranzano and Wagner, 2001b; Gopalikrishnan and Zukoski, 2004).

We suggest the generality of the onset law is because the scalings for $\tau_{min}$ are set by mechanisms for shear thinning which are independent of the mechanisms for shear thickening. Either type of shear thickening can be hidden until the stresses from shear thickening mechanisms exceed all stresses from shear thinning mechanisms (Brown et al., 2010a). This argument is simply based on which stresses are dominant, so it is not specific to a particular mechanism or to whether the shear thickening is Discontinuous or Continuous.

Each of the scaling laws for $\tau_{min}$ correspond to different dominant parameter regimes. To delineate a typical parameter regime for Discontinuous Shear Thickening in suspensions, we show each of the scalings mentioned for bounds of the shear thickening regime in Fig. 21. Since no single suspension has been used to cover the entire parameter space, we give scalings for a hypothetical suspension with some typical material properties, but note that each of the boundaries can be tuned independently depending on particle and liquid properties.

As can be seen in Fig. 21, the stress scales for Brownian motion and electrostatic interactions tend to be dominant for smaller particles in the colloid regime, while the stress scale for gravity is dominant for larger particles in the suspension regime. These scalings for $\tau_{min}$ typically meet at a size of around 10 $\mu$m depending on the values of zeta potential, density, and so on. This suggests that suspensions of particles on this size scale will tend to have the smallest values of $\tau_{min}$, as seen in Fig. 5. The minimization of $\tau_{min}$ defines an optimal particle size for shear thickening, where the largest (logarithmic) stress range for the shear thickening regime will typically be found. Since this optimal size corresponds to a balance between colloidal and suspension forces, it implies that the optimum size is fundamentally set by the colloid-suspension transition.

The maximum particle size at which shear thickening was found was about 1000 $\mu$m (Fig. 5). An upper bound is expected when $\tau_{min} \sim \Delta\rho g a$, which is set by gravity, and increases with particle size, meets with $\tau_{max} \sim \gamma/a$, which is set by surface tension, and decreases with particle size, as seen in Fig. 21. This balance corresponds to a particle capillary length scale $a \sim \sqrt{\gamma/(\Delta\rho g)}$ which differs from the usual capillary length in two ways. First, this particle capillary length depends on the density difference rather than just a liquid density. Second, this particle capillary length sets a transition between scaling regimes based on particle size rather than system size. This means surface tension effects can be seen in suspensions on much larger scales than would usually be expected based on the usual capillary length. A similar result was found by the work of Loimer et al. (2002) on free-surface flows of dense suspensions, in which they found effective stresses from surface tension scaling as $\gamma/a$.

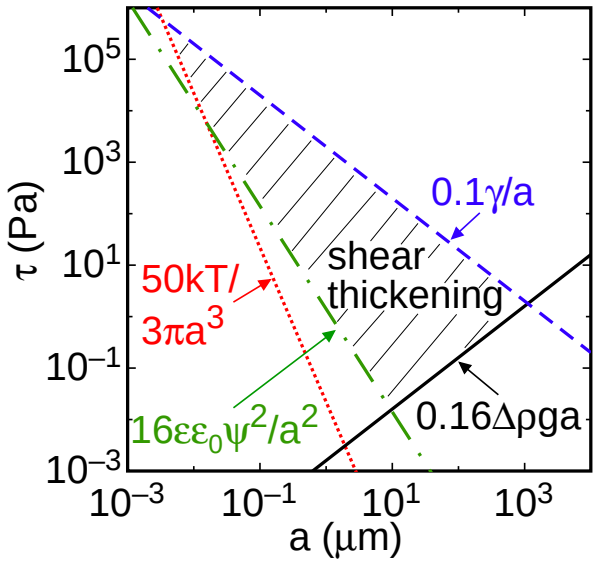


Figure 21: A rheological state diagram for a hypothetical typical suspension including all known scaling laws for shear thickening regime boundaries. It is assumed the suspension has a liquid-air interface at the boundary and the liquid wets the particles. Dotted line: Peclet number scaling due to Brownian motion taken from Maranzano and Wagner (2002). Dashed-dotted line: Electrostatic repulsion scaling based on Maranzano and Wagner (2001a) for a surface potential $\psi = 70$ mV. Dashed line: confining stress from surface tension with $\gamma = 20$ mN/m. Solid line: gravitational scaling with a density mismatch $\Delta\rho = 1$ g/mL. Since each boundary depends on different parameters, they can be tuned independently.

The particle capillary length should typically be around 1000 $\mu$m for most suspensions, in agreement with the maximum size particle found to shear thicken. While this gives a typical particle size scale above which most particles will not shear thicken in suspension, it is less tied to this size scale than the macroscopic capillary length because it depends on the density difference, so the maximum particle size could in principle be much higher for density matched suspensions.

While we have described a mechanism for shear thickening that is based on generic phenomena such as dilation, not all suspensions and colloids are reported to shear thicken. This can partly be explained by the relative importance of different stress scales. If any other particle interaction scales exceed the confining stress from surface tension, we would expect shear thinning mechanisms to be dominant over shear thickening (Brown et al., 2010a). While this is quite common in the colloidal regime, we have left some such particle interactions out of the state diagram because the corresponding scaling laws for $\tau_{min}$ are not well-established. These interactions include hydrogen bonding (Raghavan et al., 2000), depletion (Gopalikrishnan and Zukoski, 2004), or a particle-liquid surface tension (Barnes, 1989; Brown et al., 2010a). The rarity of observations of shear thickening in dense suspensions and colloids can in part be explained by the fact that many colloids fall into the regime where the stress scale of particle interactions exceeds the confining stress scale so they do not have any shear thickening regime. Another likely reason for the apparent rarity of shear thickening is that it occurs in a fairly small parameter space with a narrow range in packing fraction, so many measurements of suspension rheology simply do not cover this range.

It is provocative that cornstarch, arguably the most famous shear thickening particle, is on the optimal size scale of around 10 $\mu$m. In terms of chemical and physical properties, we have found it notable only in that it is extremely hygroscopic which implies minimal particle-liquid surface tension and consequent shear thinning effects in water (Brown et al., 2010a), which also happens to have one of the highest surface tensions of typical liquids. Cornstarch remains an inert, hard particle in aqueous suspension, in contrast with some other mass-produced powders such as flour, which gels in water at room temperature. Thus we attribute the famously strong shear thickening of cornstarch to its mass production, optimal particle size, and lack of the various interactions which produce shear thinning effects in other suspensions.

So far we have given stress scales for typical suspensions and associated with those stresses a particle size range where shear thickening can be expected. However, in most cases these were not fundamental limits and one could do better with engineered suspensions. The maximum particle size of $a \sim \sqrt{\gamma/(\Delta\rho g)}$ suggests shear thickening could be

found for much larger particles if they were density matched. If a strong shear thickening response is desired, then a high surface tension with small particles is suggested. If shear thickening is not desired, reducing the packing fraction or using softer particles are options. Many engineered suspensions are stabilized by some interparticle interaction to prevent settling. If the stress scale of the stabilizing interaction is larger than the confining stress scale, the stabilization may have the effect of hiding shear thickening, but this also increases the overall viscosity.

## 11.2 Non-local constitutive relation

We showed a constitutive relation for the shear stress with a gravitational term could describe the curvature of the shear profile (Sec. 6). That same model implied that the dramatic increase in stress associated with Discontinuous Shear Thickening could not be attributed to a local shear rate dependence from viscous stresses (whose contribution appeared to be relatively constant in the shear thickening regime). Instead, we showed in Sec. 7 that the shear stress was coupled to the normal stress, which could be characterized by an effective friction coefficient $\mu$ between them. In turn, the normal stress was shown to come from the restoring force of the boundary against dilation (Secs. 9, 10). We can now fully express the constitutive relation between local shear stress $\tau_l$ and local shear rate $\dot{\gamma}_l$ based on Eq. 3 with the "constant" term $\tau_c$ explicitly separated into the confining stress contribution as well as a constant contribution from interparticle interactions $\tau_{int}$:

$$\tau_l = \eta_\nu(\phi)\dot{\gamma}_l f(Re) + \tau_g h/d + \mu\tau_{conf}(\delta) + \tau_{int} \tag{8}$$

where $\tau_{conf}(\delta) = \delta k/a^2$ for a linear elastic boundary with per-particle stiffness $k$ (Fig. 20), and $f(Re) = 1$ in the viscous regime where $Re < Re_c \sim 100$ and $f(Re) = Re/Re_c$ in the fully inertial regime where $Re \gg Re_c$ (Sec. 4). In contrast to typical hydrodynamic constitutive laws, this constitutive law is non-local because the normal stress term depends on the global dilation $\delta$ which causes a restoring force that transmits stress through the system via force chains. It is also notable that the boundary conditions can have an uncommonly large effect on the normal stress term because it is due to a confining stress.

The major success of this constitutive relation is that it allows for simple estimates of the stress scales $\tau_{min}$, $\tau_{max}$, and $\tau_j$, and consequently whether a system will shear thicken. It can also simply explain observations under different measuring geometries and boundary conditions, for example in suspensions where gravity is dominant. In a parallel plate geometry, we found settling suspensions to be jammed, i.e. have zero shear rate, at stresses below $\tau_{min} = \tau_g a/d$, and at higher stresses have a shear band whose width increased with $\tau$ according to Eq. 8 (Secs. 5, 6). In a Couette geometry where the moving wall is on the side, any density mismatch was found to result in a yield stress scaling as $\tau_g \sim \Delta\rho g H$ (Fall et al., 2009), which is also described by Eq. 8 since the depth $h$ at the moving wall is not everywhere zero.

The term in the constitutive law responsible for shear thickening is the normal stress term, which increases dramatically when dilation causes particles to push against the boundary, resulting in a restoring force that acts as a confining stress (Fig. 15, 20). The significance of the normal stress term becomes even clearer when we consider some of the cases that did not shear thicken. In cases without any normal stress, as in the normal force control measurements (Fig. 9), this term is zero and consequently there is no shear thickening. For granular materials with a yield stress, normal forces can be the result of particles jammed against confining boundaries, or due to gravity in dry granular flows. In these cases, the normal stress term is still dominant, but it is relatively independent of shear rate, which is why a yield stress and shear thinning are found instead of shear thickening. In other yield stress fluids, the yield stress may come from particle interactions, which could be represented by $\tau_{int}$ instead of a normal stress term, but the end result is a yield stress and shear thinning in either case (Brown et al., 2010a).

We cannot yet fully solve the constitutive relation in Eq. 8 because dilation in suspensions is not yet well-characterized. Specifically, the slope of viscosity curves in the shear thickening regime should depend on how dilation varies with shear rate, stresses, and packing fraction. Dilation in suspensions at non-zero shear rates occurs at packing fractions significant lower than for dry grains in the quasi-static limit (Onoda and Liniger, 1990; Jerkins et al., 2008; Kabla and Senden, 2009). This suggests hydrodynamic models will be useful for understanding dilation in suspensions. As an example, simulations have shown that a pair of particles compressed together by viscous forces can rotate in the plane of the shear gradient together which should cause the structure to dilate (Dratler, 1997). O'Brien and Mackay (2000) suggested a mechanism by which hydrodynamically-induced clusters could lead to dilation, but this has yet to be investigated.

Fig. 15 shows a single scaling for the dilation with shear stress through the transition at $\tau_{max}$. Since the stress/shear-rate curve corresponds to Discontinuous Shear thickening, this implies the dilation $\delta$ increases rapidly with shear rate in the shear thickening regime, then increases less rapidly above $\tau_{max}$. Suggestively, this rapid increase of dilation with shear rate corresponds to the regime where the shear band is widening (Fig. 6), and the dilation increases less rapidly once the shear band stops widening. We cannot say for sure that these observations are connected, but it may be that the rapid increase in dilation is required to involve more layers of particles in the shear flow.

It is interesting to note that the local shear-rate dependence in Eq. 8 is inherently shear thinning in the low-$Re$ regime where Discontinuous Shear Thickening is observed. Similarly, we found that the local viscosity in the bulk obtained from shear profile measurements corresponded to shear thinning (Figs. 6,7), even for a global mechanical response that corresponded to shear thickening. The explanation for this apparent contradiction is that most of the shear stress is due to frictional contacts and thus comes from the normal stress, which can vary greatly with the boundary conditions. It is only because granular materials dilate under shear against an elastic boundary that the global response is shear thickening. From a hydrodynamic point of view, the large significance of the boundary conditions and difference between local and global results is unusual, as it is more typical for the boundary conditions to play a smaller role, requiring only perturbative corrections to translate between the local and global rheology. One of the surprising consequences of this is that characterizing rheology based solely on local, shear-rate dependent constitutive laws or local viscosities in the bulk would miss the dramatic phenomenon associated with Discontinuous Shear Thickening.

## 11.3 Confining stress in other systems

In this section we consider the confining stress scale for granular systems other than suspensions in contact with air and what that says about why they do or do not shear thicken.

We found the upper end of the shear thickening regime $\tau_{max}$ to be set by the confining stress which comes from the restoring force when grains dilate against a boundary, either from surface tension when there is a liquid-air interface (Figs. 16, 17) or by the stiffness of the wall when all boundaries are solid (Fig. 20). In the discussions of the confining stress so far, the most compliant boundary set the response. This is because the stiffness of a system of several elements with very different stiffnesses in series will generally be determined by the most compliant element in the series. In some systems, the particles could be the most compliant element. This regime would be relevant when all of the walls are very hard, and it has been proposed such a regime may be reached for small colloidal particles where the confining stress from surface tension is larger (Wagner and Brady, 2009). If there is a lubrication layer of liquid between gaps, the maximum confining stress would be coupled to the viscosity because the particle compression depends on the stress in the lubrication layer. For solid contacts between elastic spheres, the confining stress would be limiting by a scale of $(\delta/R)^{3/2}E_p$ where $E_p$ is the compressional modulus of the particles and $\delta/R$ corresponds to the compressional strain on the sample. The 3/2 power comes from the contact between two spherical surfaces as opposed to the power of 1 for flat surfaces. For the hard particles we used with $E_p \sim 10^{10}$ and $\delta \approx 10^{-2}$, this scale is of order $10^7$ Pa, which is much stiffer than the liquid-air interface. Stresses up to about $10^7$ Pa have been observed in the shear thickening regime for silica particles in compressional flows with solid walls (Lim et al., 2010), which is consistent with the idea that much larger confining stresses can be reached for hard walls. On the other hand, if the particles are extremely soft, the confining stress may be below $\tau_{min}$. This seems to be the case in a suspension of soft gel particles with modulus on the order $10^4$ Pa in which only shear thinning was observed instead of shear thickening as the jamming transition was approached (Nordstrom et al., 2010). In such cases where the confining stress comes from solid walls or particles, we expect much larger particles to be able to shear thicken, as the effect would no longer limited by the strength of surface tension on large scales.

Dry grains in an open container are not known to shear thicken. When they shear they dilate but there is no interface to provide a restoring force. There is a confining stress from gravity, but since that also sets the scale of the yield stress (Fig. 5), only shear thinning should be expected. It is only when we provide a confining stress by enclosing the system with solid walls that shear thickening can be found for dry grains (Fig. 18). It is clear now that one of the important differences between dry and wet grains is that the surface tension of the liquid provides a confining stress. This emphasizes the fact that not only is dilation required for shear thickening, but also that it must be partially frustrated by a restoring force from the boundary, otherwise there is no confining stress.

Some measurements of sheared dense suspensions found only inertial scaling rather than Discontinuous Shear Thickening (Bagnold, 1954). Notably, those experiments were done in an enclosed system but with a rubber sheet in the wall to allow dilation of the suspensions and a liquid reservoir to allow liquid to fill the gaps enlarged by dilation. Thus it seems likely that the rubber sheet was soft enough that its compression did not provide a significant confining stress in excess of the inertial contribution to the stress. In other words, if the enclosure is very compliant and allows dilation without producing a confining stress, then we expect behavior similar to an open system. This suggests a possible method for greatly reducing the resistance in pipe flow of dense suspensions, namely to use compliant walls and a liquid reservior.

A closed system with very hard walls is expected to cause the grains to jam as there is no room for dilation and the hard walls would be able to apply enough stress to hold particles in place. This effect has been seen for hard disks in a hard-walled system just below the onset of jamming based on uniform compression. The disks contacted each other via force chains when sheared quasi-statically, i.e. the system jammed rather than shear thickened (Zhang et al., 2008). In contrast to the case for suspensions with a liquid-air interface, the yield stress above the jamming transition with hard walls scales with the particle modulus as the particles compress against each other, which is

the most compliant component of the system if the walls are harder. This results in a different scaling for the yield stress with packing fraction, since with hard walls the confining stress increases as the system is further compressed to higher packing fractions (O'Hern et al., 2003), while for a suspension the confining stress is limited by the scale $\gamma/a$ regardless of further compression.

Foams are another system used for jamming experiments with soft particles. Rheologically they are generally found to shear thin, even in confined volumes. In jammed foams, the yield stress is observed to be on the scale of $\tau_y \approx 0.05\gamma/a$ (Gardiner et al., 1998). This is the same relation we find for $\tau_{max}$ in response to dilation or for jammed suspensions due to the deformation of the liquid-air interface. Since bubbles are very soft, they will be the limiting factor that determines the confining stress. Since this stress will be very low, it seems unlikely that it can exceed attractive interactions considering they both come from surface tension. As a result Discontinuous Shear Thickening should not be expected. Similarly, emulsions are very soft particles with stiffness set by surface tension, in which Discontinuous Shear Thickening is not observed.

Molecular liquids are classic Newtonian fluids, yet on a molecular level they are a disorganized collection of particles. While molecular liquids exhibit an apparent shear thickening due to inertial effects at high Reynolds numbers, they do not generally exhibit Discontinuous Shear Thickening. In slow, unidirectional shear flows of bulk molecular liquids there are no normal forces. This implies liquid molecules in bulk can shear past each other without confining stresses, and thus Discontinuous Shear Thickening should not be expected.

An important feature that makes granular materials distinct from molecular liquids and foams is that only the hard grains dilate under shear. This dilation leads to a stress determined by the boundary condition. Soft or otherwise unconfined particles can shear without a significant confining stress, which can result in a Newtonian rheology if the particles are not strongly interacting. If particle interactions are dominant, shear thinning is usually found. Only confined and sufficiently hard particles can dilate against a boundary and produce enough confining stress to result in Discontinuous Shear Thickening.

While simulations of suspension have successfully modeled Continuous Shear Thickening effects, so far most have failed to produce the large, dramatic stress increases associated with Discontinuous Shear Thickening (Brady and Bossis, 1985; Melrose et al., 1996; Farr et al., 1997; Bergenholtz et al., 2002; Melrose and Ball, 2001a, 2004b; Grebenkov, 2008). These simulations have included viscous interactions as well as various interparticle interactions. Most have focused on bulk behavior, usually using periodic boundary conditions such as Lees-Edwards to avoid dealing with boundary effects. Now that we have recognized that the boundary conditions and especially the confining stress are important, it seems likely that many of these simulations did not find Discontinuous Shear Thickening because of their treatment of the boundary conditions. The one simulation we are aware of that has produced Discontinuous Shear Thickening was a molecular dynamics simulation of two-dimensional granular shear flow with frictional contacts between particles but no liquid or viscous interactions (Otsuki and Hayakawa, 2010). Besides a steep $\tau(\dot{\gamma})$ at packing fractions just below the jamming transition, the scale of the normal and shear stresses was found to be set by the particle modulus, which in that simulation was the only scale that could set a confining stress. This may be a minimal model for Discontinuous Shear Thickening in two dimensions since it includes particle-particle contacts with a restoring force, but leaves out the liquid.

While we have described a mechanism for shear thickening due to confining stresses in shear flows, the same principle could apply to extensional and compressional flows because stresses tend to be easily redistributed in different directions along particle contacts in granular flows. Visible dilation at the surface was seen to correspond to shear thickening in an extensional flow(Smith et al., 2010). The maximum stress in the shear thickening regime $\tau_{max}$ in extensional flows (Chellamuthu et al., 2009; Bischoff White et al., 2010) has been found to be about an order of magnitude higher $\tau_{max}$ based on shear measurements, but this could still be consistent with a scale of $\gamma/a$. While these isolated result are promising, our model has not yet been extensively tested in extensional flows.

## 11.4 Connection to solid mechanics

We showed that the scale of the stress response of Discontinuous Shear Thickening is set by a confining stress. A close analogy can be made to other systems, for example in the field of soil mechanics. In typical soil mechanics tests, a granular material is compressed or sheared under some known applied confining pressure. This confining pressure determines the scale of the stress response against shear or compression (Lambe and Whitman, 1969). An important distinction is that soil mechanics tests are generally done with a controlled fixed confining stress, so there is no shear thickening transition.

One lesson to take away from soil mechanics is that even though the global response of the system is set by the boundary conditions, the scale of the stress response is not dependent on sample size or shape. This is because forces will transmit throughout the bulk across particle contacts, and forces must balance across the system, regardless of how far across the bulk is. This makes stress the appropriate size-independent force scale as in other continuum systems. In Discontinuous Shear Thickening suspensions, the same qualitative behavior has been seen from as few as 2 particle layers (Brown et al., 2010b) to tens of thousands of layers (Maranzano and Wagner, 2001a). Quantitatively,

the significance of the surface area to volume ratio can be checked by varying the gap size in a parallel plate geometry for a fixed volume of sample. For such measurements at constant shear rate, we found that the percentage change in stress was $(0.20 \pm 0.22)\%$ over a range where the surface area changed by 17% (Brown et al., 2010b). This is consistent with with a shear stress independent of surface area and inconsistent with a stress proportional to surface area. Furthermore, similar results have been found when comparing Couette cell measurements with parallel plate measurements (Fall et al., 2008). Together, these observations support the argument that the relevant stress scale for shear thickening is not dependent on the system size or shape.

It has been suggested that shear thickening is a form of jamming (Farr et al., 1997; Cates et al., 1998; Hébraud and Lootens, 2005; Maranzano and Wagner, 2001a; Fall et al., 2008). Visible shear in and above the shear thickening regime shows that shear thickening is not jamming in the sense of being associated with a yield stress or static structures (Figs. 6, 7, 14). Below the onset of shear thickening, the particles may be settled or stuck together by attractions; in either case this corresponds to a locally static structure, and in many cases the system is jammed with a yield stress below the shear thickening regime. The shear thickening regime can be where more of the particles become involved in shear, i.e. becoming unjammed in the above sense, and it is the resulting dilation against the boundaries under shear which causes the shear stress to increase dramatically.

One connection between Discontinuous Shear Thickening and jamming comes from the observation that they are controlled by the same critical packing fraction $\phi_c$ (Brown and Jaeger, 2009). The shear rate at the onset of shear thickening goes to zero in the limit of $\phi_c$, suggesting the limiting case of shear thickening corresponds to a yield stress, i.e. a jammed state, which is also what is found on the other side of $\phi_c$ (Brown and Jaeger, 2009). The other connection between Discontinuous Shear Thickening and jamming, which was hinted at by Holmes et al. (2003, 2005) and Melrose and Ball (2004b), comes from the stress response, whose scales $\tau_{max}$ and $\tau_j$, respectively, are set by a confining stress due to the penetration of particles through the liquid-air interface in each case and which is transmitted through the system via force chains. This occurs with dilation under shear for Discontinuous Shear Thickening (Figs. 14, 15), and at rest for jammed suspensions (Figs. 11, 12). In terms of the stress response, Discontinuous Shear Thickening could be considered to be a dynamic extension of jamming, but so far there is not yet a formalism for describing jamming in non-static systems.

## 11.5 Summary of the mechanism for Discontinuous Shear Thickening

Based on the proposed mechanism for shear thickening, the requirements for Discontinuous Shear Thickening, not necessarily limited to suspensions, can be stated as:

1. Dilation: The system must dilate when sheared. This usually requires a high packing fraction, close to the jamming transition.
2. Confining stress: There must be a confining stress that provides a strain-dependent restoring force against dilation. This confining stress can come from surface tension at a liquid-air interface, the walls surrounding the system, or the particle stiffness.
3. Dominance of confining stress: The confining stress from the most compliant boundary must significantly exceed all stresses that prevent granular shear and dilation, such as interparticle interactions or gravity. Otherwise, there is not enough stress increase from dilation to result in a positive slope on a viscosity curve and the global rheology may be shear thinning instead.

Here we compare this mechanism to others that have been proposed. Hoffman (1982) argued that "[Discontinuous Shear Thickening] will occur in concentrated suspensions whenever the particles can segregate into layers parallel to planes of constant shear, but are constrained from free rotation at levels below some critical level of stress." Our model is in agreement with that of Hoffman (1982) in which the onset stress is determined by a point where the shear stress is large enough to shear particles in such a way to cause dilation. Hoffman (1982) argued for the the same onset scaling law with the stress scale corresponding to the interaction between zeta potentials of neighboring particles shown in Fig. 21. Our proposed scaling for the confining stress $\tau_{max}$ gives the scale measured by Hoffman (1972), whose data is included in Fig. 17. While Hoffman observed an order-disorder transition along with Discontinuous Shear Thickening, it was shown that such a transition is not necessary (Maranzano and Wagner, 2002; Egres and Wagner, 2005; Egres et al., 2006), which suggests the order-disorder transition is not the key to explaining the stresses. Rather, an we suggest the order-disorder transition may be a cause of volumetric dilation, considering that disordered packings tend to be less space-efficient than ordered packings. While Hoffman did not report direct evidence for or against dilation, our model provides the most thorough explanation for the stresses observed in those experiments with an order-disorder transition and thus provides a likely explanation for Discontinuous Shear Thickening in those systems.

Many other papers have supported a hydrocluster mechanism (Brady and Bossis, 1985; Maranzano and Wagner, 2001a; Shenoy and Wagner, 2005) based on the ability of those models to predict some of the scalings for the onset $\tau_{min}$ shown in Fig. 21. We have argued that these onset scalings can be more simply understood in terms of dominant

stress scales which are not dependent on a base hydrodynamic model, and can apply to any mechanisms for shear thickening including hydrodynamic effects (Bergenholtz et al., 2002) or aggregation (Osuji et al., 2008). Additionally, our proposed mechanism can also explain the scaling for $\tau_{max}$, as well as explaining the otherwise unusual dependence of the rheology on the boundary conditions.

Our model predicts the stress scales $\tau_{min}$ and $\tau_{max}$ that bound the shear thickening regime, both in suspensions and colloids, a success that has not been achieved by any other model for shear thickening. Thus, our model provides the most thorough explanation for the stresses observed in Discontinuous Shear Thickening in either suspensions or colloids. However, the dilational mechanism has not yet been investigated in detail for colloids.

# 12 Conclusions

In this paper we proposed and tested a mechanism for Discontinuous Shear Thickening, which we briefly summarize here. The onset of shear thickening at $\tau_{min}$ occurs when the shear stress overcomes stresses holding the grains together and they start to shear relative to each other (Figs. 5, 6, 7). This shear causes the grain packing to dilate (Figs. 13, 14). Dilation in turn causes the particles to push against the boundary, typically the liquid-air interface for suspensions open to the air, which pushes back with a restoring force to produce a confining stress on the suspension (Figs. 15, 16, 17). The resulting normal stresses are transmitted through the packing via frictional interactions (Figs. 8, 9,10), resulting in a rapid increase in shear stress with shear rate corresponding to Discontinuous Shear Thickening.

Using these results, we listed the requirements for Discontinuous Shear Thickening to be dilation under shear and a confining stress in response to dilation which exceeds all stress scales corresponding to other types of particle interactions (Sec. 11.5). We delineated the scaling laws for $\tau_{min}$ and $\tau_{max}$ that set the parameter range of the shear thickening regime in both suspensions and colloids (Fig. 21). We introduced a non-local constitutive relation which is locally shear thinning, but where Discontinuous Shear Thickening comes out of a frictional term from the confining stress at the boundary which depends on the global dilation (Sec. 11.2).

We generalized this shear thickening mechanism to other sources of a confining stress by showing that, when instead grains are confined by solid walls and have no liquid-air interface, $\tau_{max}$ is set by the stiffness of the most compliant boundary (Figs. 18, 19, 20).

We elucidated the relationships between Discontinuous Shear Thickening and other phenomena. We distinguished Discontinuous Shear Thickening from inertial hydrodynamic effects by showing that a Reynolds number characterizes inertial effects (Figs. 3, 4), and that this number is small at the low shear rates where Discontinuous Shear Thickening is observed. We showed that similarities in the mechanical properties of Discontinuous Shear Thickening and jammed suspensions come from the confining stress due to the penetration of particles through the liquid-air interface (Figs. 11, 12, 14). Similarities to the mechanics of dry granular flows and soils stem from the frictional interactions between particles under confinement (Fig. 9)

# 13 Acknowledgements

We thank S. Nagel, T. Witten, and W. Zhang for thoughtful discussions. We thank Marc Miskin for designing the optical setup used in the shear profile videos. We thank Franco Tapia Uribe for taking preliminary shear profile measurements. We thank Trevor Martin for machining the solid wall setup for the rheometer. This work was supported by DARPA through Army grant W911NF-08-1-0209 and by the NSF MRSEC program under DMR-0820054.

# 14 Appendix: calculation of confining stress at liquid-air interface from dilation

To connect the confining stress at the liquid-air interface to the measured dilation $\delta$, a model is needed for the interface geometry. For simplicity we will assume spherical particles with a contact angle $\theta = 0$ at the liquid-solid-air contact line since to obtain shear thickening the liquid must wet the particles. For this contact angle the interface geometry is equivalent to a sphere of air of radius $r$ in contact with particles at the surface. We will calculate the geometry for a characteristic radius of curvature as if it is the same at each interstice between particles, and use these mean single-particle calculations as an estimate for the surface as a whole, ignoring variations in the surface curvature. The point of contact is defined by an angle $\alpha$ relative to horizontal as shown in Fig. 22. The packing fraction of particles on the two dimensional surface will be represented by $\phi_{2D}$. As an estimate we will use the value $\phi_{2D} = 0.84$ which corresponds to random close packing in two dimensions (O'Hern et al., 2002). This geometry gives

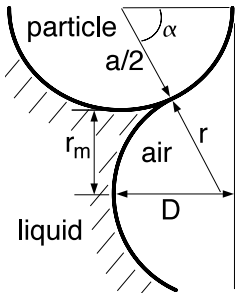


Figure 22: Dimensions used for calculation of relationship between dilation $\delta$ and confining stress due to surface tension at a liquid-air interface with radius of curvature $r$.

enough constraints to relate the radius of curvature $r$ to the contact angle. The dilation $\delta$ can be connected to this geometry using conservation of volume. The confining stress scale from surface tension can then be calculated as proportional to $\gamma/r$ as a function of $\delta$.

From the geometry in Fig. 22, the vertical components of the dimensions can be used to relate the radius of curvature to the contact angle

$$r \sin\alpha = \frac{a}{2}(1 - \sin\alpha) + r_m \ . \tag{9}$$

The minimum radius of curvature $r_m$ comes from the minimum radius of the insterstitial gap between particles. At an interstice between 3 particles in contact, this is $r_m/a = \sqrt{1/3} - 1/2 \approx 0.26$ in three dimensions, while in two dimensions $r_m$ would be zero. The mean confining stress is modeled as

$$\tau_{conf} \sim \frac{\gamma}{r}(1 - \phi_{2D} \sin^2\alpha) \tag{10}$$

where $1 - \phi_{2D} \sin^2\alpha$ is the fractional cross-sectional area around the outer edge covered by the liquid-air interface.

Next, we relate the dilation $\delta$ to $\alpha$. Conservation of volume requires that the dilation match the enclosed volume of air per particle $\Delta V$ up to the maximum penetration of the particle when using the initial condition that the surface is flat ($r = \infty$) when $\delta = 0$:

$$\delta = \frac{4\phi_{2D}\Delta V(r,\alpha)}{\pi a^2} \ . \tag{11}$$

The volume $\Delta V$ can be calculated as

$$\Delta V = 2V_{cap} + V_i \tag{12}$$

where $V_{cap}$ is the volume of a spherical cap interior to the point of contact (of which there are 2 per particle)

$$V_{cap} = \frac{\pi r^3}{3}(1 - \cos\alpha)^2(2 + \cos\alpha) \tag{13}$$

and $V_i$ comes from integrating the fluid volume in the mean surface normal direction from the furthest point of penetration of the particle up to the point of contact:

$$V_i = \int_0^\alpha \frac{\pi a^3}{4} \sin\alpha' \left[\frac{1}{\phi_{2D}} - \sin^2\alpha'\right] d\alpha' = \frac{\pi a^3}{4}\left[\frac{1 - \cos\alpha}{\phi_{2D}} - \frac{\cos(3\alpha) - 9\cos\alpha + 8}{12}\right] \ . \tag{14}$$

With Eqns. 9, 10, and 11 relating $\tau_{conf}$, $\delta$, $r$, and $\alpha$, they can be solved numerically to obtain a relationship between $\delta$ and $\tau_{conf}$, with the result shown in Fig. 15.

These equations may be valid until the point where the contact line reaches the 2nd layer of particles from the surface, beyond which extra contact lines are made. This starts when the maximum penetration, defined in Fig. 22 as $D = (a/2 + r)(1 - \cos\alpha)$, reaches $\sqrt{3}a/2$ which corresponds to the layer width for a hexagonal packing. This limit is shown as the dashed line in Fig. 15.

# References

Bagnold, R.A., "Experiments on a gravity-free dispersion of large solid spheres in a newtonian fluid under shear," Proc. Royal Soc. London A: Math. and Phys. Sci. **225** (1160), 49 (1954).

Barnes, H.A.,"Shear-thickening ("Dilatancy") in suspensions of nonaggregating solid particles dispersed in Newtonian liquids," J. Rheology **33** (2), 329 (1989).

Bender, J. and N. Wagner, "Reversible shear thickening in monodisperse and bidisperse colloidal dispersions," J. Rheology **40** (5), 899 (1996).

Bergenholtz, J., J.F. Brady, and M. Vicic, "The non-Newtonian rheology of dilute colloidal suspensions," J. Fluid Mech. **456**, 239 (2002).

Bertrand, E., J. Bibette, and Véronique Schmitt, "From shear thickening to shear-induced jamming," Phys. Rev. E **66**, 060401(R) (2002).

Bocquet, L., W. Losert, D. Schalk, T.C. Lubensky, and J.P. Gollub, "Granular shear flow dynamics and forces: experiment and continuum theory," Phys. Rev. E **65**, 011307 (2001).

Boersma, W.H., P.J. M. Baets, J. Laven, and H.N. Stein, "Time-dependent behavior and wall slip in concentrated shear thickening dispersions," J. Rheol. **35** (6), 1093 (1991).

Boersma, W.H., J. Laven, H.N. Stein, "Shear thickening (dilatancy) in concentrated dispersions," AIChE **36**, 321 (1990).

Brady, J.F. and G. Bossis, "The rheology of concentrated suspensions of spheres in simple shear flow by numerical simulation," J. Fluid Mech. **155**, 105 (1985).

Brady, J.F. and M. Vicic, "Normal stresses in colloidal dispersions," J. Rheol. **39** (3), 545 (1995).

Brown, E and H.M. Jaeger, "Dynamic jamming point for shear thickening suspensions," Phys. Rev. Lett **103** 086001 (2009).

Brown, E., N. A. Forman, C. S. Orellana, H. Zhang, B. W. Maynor, D. E. Betts, J. M. DeSimone, and H. M. Jaeger, "Generality of shear thickening in suspensions," Nature: Materials **9** (3) 220-224 (2010a).

Brown, E. H. Zhang, N. A. Forman, B. W. Maynor, D. E. Betts, J. M. DeSimone, and H. M. Jaeger, "Shear thickening in densely packed suspensions of spheres and rods confined to few layers," J. Rheol. **54** (5) 1023 (2010b).

Cates, M.E., R. Adhikari, and K. Stratford, "Colloidal arrest by capillary forces," J. Phys.: Condens. Matter **17**, S2771 (2005).

Cates, M.E., M.D. Haw and C.B. Holmes, "Dilatancy, jamming, and the physics of granulation," J. Phys: Condens. Matter **17** S2517 (2005).

Cates, M.E., J.P. Wittmer, J.-P. Bouchaud, and P. Claudin, "Jamming, force chains, and fragile matter," Phys. Rev. Lett. **81** (9), 1841 (1998).

Chellamuthu, M., E.M. Arndth, and J.P. Rothstein, "Extensional rheology of shear thickening nanoparticle suspensions," Soft Matter **5** (10), 2117 (2009).

Corwin, E.I., H.M. Jaeger and S.R. Nagel, "Structural signature of jamming in granular media," Nature **435**, 1075 (2005).

Donnelly, R.J. and N.J. Simon, "An empirical torque relation for supercritical flow between rotating cylinders," J. Fluid. Mech. **7**, 401 (1960).

Dratler, D.I., W.R. Schowalter, and R.L. Hoffman, "Dynamic simulation of shear thickening in concentrated colloidal suspensions," J. Fluid Mech. **353**, 1 (1997).

Egres, R.G. and N. J. Wagner, "The rheology and microstructure of acicular precipated calcium carbonate colloidal suspensions through the shear thickening transition," J. Rheol. **49** (3), 719 (2005).

Egres, R.G., F. Nettesheim, and N.J. Wagner, "Rheo-SANS investigation of acicular-precipitated calcium carbonate colloidal suspensions through the shear thickening transition," J. Rheol. **50** (5), 685 (2006).

Fall, A., F. Bertrand, G. Ovarlez, and D. Bonn, "Yield stress and shear banding in granular suspensions," Phys. Rev. Lett. **103**, 178301 (2009).

Fall, A., N. Huang, F. Bertrand, G. Ovarlez, and D.Bonn, "Shear thickening of cornstarch suspensions as a reentrant jamming transition," Phys. Rev. Lett. **100**, 018301 (2008).

Fall, A., A. Lemaître, F. Bertrand, D. Bonn, G. Ovarlez, "Continuous and discontinuous shear thickening in granular suspensions," submitted to Phys. Rev. Lett. (2010).

Farr, R.S., J.R. Melrose, and R.C. Ball, "Kinetic theory of jamming in hard-sphere startup flows," Phys. Rev. E **55** (6), 7203 (1997).

Frith, W.J., P. d'Haene, R. Buscall, J. Mewis, "Shear thickening in model suspensions of sterically stabilized particles," J. Rheology **40** (4), 531 (1996).

Gallay, W. and I.E. Puddington, Can. J. Res. C **21**, 179 (1943).

B.S. Gardiner, B.Z. Dlugogorski, G.J. Jameson, R.P. Chhabra, J. Rheol **42** (6), 1437 (1998).

Goldman, A.J., R.G. Cox, and H. Brenner, "Slow viscous motion of a sphere parallel to a plane wall – Couette flow," Chem. Eng. Sci. **22**, 653 (1967).

Gopalakrishnan, V., and C.F. Zukoski, "Effect of attractions on shear thickening in dense suspensions," J. Rheol. **48** (6), 1321 (2004).

Grebenkov, D.S., M.P. Ciamarra, M. Nicodemi, and A. Coniglio, "Flow, ordering, and jamming of sheared granular suspensions," Phys. Rev. Lett. **100**, 078001 (2008).

Hébraud, P. and D. Lootens, "Concentrated suspensions under flow: shear-thickening and jamming," Mod. Phys. Lett. B **19** (13-14), 613 (2005).

Hoffman, R. L., "Discontinuous and dilatant viscosity behavior in concentrated suspensions: observation of a flow instability," Trans. Soc. Rheol. **16**, 155 (1972).

Hoffman, R.L., "Discontinuous and dilatant viscosity behaivior in concentrated suspensions II. Theory and experimental tests," J. Colloid Interface Sci. **46** 491 (1974).

Hoffman, R.L., "Discontinuous and dilatant viscosity behavior in concentrated suspensions III: necessary conditions for their occurrence in viscometric flows," Advances in Colloid and Interface Sci. **17** 161 (1982).

Hoffman, R.L., "Explanations for the cause of shear thickening in concentrated colloidal suspensions," J. Rheol. **42** (1), 111 (1998).

Holmes, C.B., M. Fuchs, and M.E. Cates, "Jamming transitions in a schematic model of suspension rheology," Europhys. Lett. **63** (2), 240 (2003).

Holmes, C.B., M. E. Cates, M. Fuchs, and P. Sollich, "Glass transitions and shear thickening suspension rheology," J. Rheol. **49** (1), 237 (2005).

Jaeger, H.M., S.R. Nagel, R.P.Behringer, "Granular, solids, liquids, and gases," Rev. Mod. Phys. **68**, 1259 (1996).

Janssen, Z., "Experiments on corn pressure in silo cells," Verein Deutsch. Ing. **39**, 1045 (1895).

Jerkins, M., M. Schröter, H.L. Swinney, T.J. Senden, M. Saadatfar, T. Aste, "Onset of mechanical stability in random packings of frictional spheres," Phys. Rev. Lett. **101**, 018301 (2008).

Jolly, M.R. and J.W. Bender, US patent application No. 20060231357.

Jomha, A.I. and P.A. Reynolds, "An experimental study of the first normal stress difference – shear stress relationship in simple shear flow for concentrated shear thickening suspensions," Rheol. Acta **32** 457 (1993).

Kabla, A.J. and T.J. Senden, "Dilatancy in slow granular flows," Phys. Rev. Lett. **102**, 228301 (2009).

Knight, J.B., C.G. Fandrich, C.N. Lau, H.M. Jaeger, and S.R. Nagel, "Density relaxation in a vibrated granular material," Phys. Rev. E **51** (5), 3957 (1995).

Koos, E. and N. Willenbacher, "Capillary forces in suspension rheology," Science **331** (6019), 897 (2011).

Kulkarmi, P.M., and J.F. Morris, "Suspension properties at finite Reynolds number from simulated shear flow," Phys. Fluids **20**, 040602 (2008).

Lambe, T.W. and R.V. Whitman, (1969) Soil Mechanics (John Wiley and Sons, New York).

Larsen, R.J., J.-W. Kim, C. F. Zukoski, and D.A. Weitz, "Elasticity of dilatant particle suspensions during flow," Phys. Rev. E **81**, 011502 (2010).

Laun, H.M., "Normal stresses in extremely shear thickening polymer dispersions," J. Non-Newtonian Fluid Mech **54** 87 (1994).

Laun, H.M., R. Bung, and F. Schmidt, "Rheology of extremely shear thickening polymer dispersions (passively viscosity switching fluids)," J. Rheol. **35** (6), 999 (1991).

Lee, Y.S. and N.J. Wagner, "Rheological properties and small-angle neutron scatting of a shear thickening, nanoparticle dispersion at high shear rates," Ind. Eng. Chem. Res. **45**, 7015 (2006).

Lee, Y.S., E.D. Wetzel, and N.J Wagner, "The ballistic impact characteristics of Kevlar-woven fabrics impregnated with a colloidal shear thickening fluid," J. Materials Sci. **38**, 2825 (2003).

Lenoble, M., P. Snabre, and B. Pouligny, "The flow of a very concentrated slurry in a parellel-plate device: influence of gravity," Phys. Fluids **17**, 073303 (2005).

Lim, A.S., S.L. Lopatnikov, N.J. Wagner, and J.W. Gillespie, "An experimental investigation into the kinematics of a concentrated hard-sphere colloidal suspension during Hopkinson bar evaluation at high stresses," J. Non-Newtonian Fluid Mech. **165** (19), 1342 (2010).

Liu, A.J. and S. R. Nagel, "Jamming is not just cool any more," Nature **396**, 21 (1998).

Loimer, T., A. Nir, and R. Semiat, " Shear-induced corrugation of free interfaces in concentrated suspensions," J. Non-Newtonian Fluid Mech. **102**, 115 (2002).

Lootens, D., H. Van Damme, and P. Hébraud, "Giant stress fluctuations at the jamming transition," Phys. Rev. Lett. **90**, No. 17, 178301 (2003).

Lootens, D., H. Van Damme, Y. Hémar, and P. Hébraud, "Dilatant flow of concentrated suspensions of rough particles," Phys. Rev. Lett. **95**, 268302 (2005).

Majmudar, T.S. and R.P. Behringer, "Contact force measurements and stress-induced anisotropy in granular materials," Nature **435**, 1079 (2005).

Maranzano, B.J., and N. J. Wagner, "The effects of particle size on reversible shear thickening of concentrated colloidal suspensions," J. Chem. Phys. **114** (23), 10514 (2001a).

Maranzano, B.J. and N. J. Wagner, "The effects of interparticle interactions and particle size on reversible shear thickening: hard-sphere colloidal dispersions," J. Rheol. **45** (5), 1205 (2001b).

Maranzano, B.J. and N. J. Wagner, "Flow-small angle neutron scattering measurements of colloidal dispersion microstructure evolution through the shear thickening transition," J. Chem. Phys. **117** (22), 10291 (2002).

Melrose, J.R. and R.C. Ball, "Continuous shear thickening transitions in model concentrated colloids – the role of interparticle forces," J. Rheol. **48** (5), 937 (2004a).

Melrose, J.R., R. C. Ball, "Contact networks in continuously shear thickening colloids," J. Rheology **48** (5), 961 (2004b).

Melrose, J.R., J.H. van Vliet, and R.C. Ball, "Continuous shear thickening and colloid surfaces," Phys. Rev. Lett. **77** (22), 4660 (1996).

Metzner, A.B., and M. Whitlock, "Flow behavior of concentrated (Dilatant) suspensions," Trans. Soc. Rheol. **11**, 239 (1958).

Mueth, D.M., G.F. Debregeas, G.S. Karczmar, P.J. Eng, S.R. Nagel, and H.M. Jaeger, "Signatures of granular microstructure in dense shear flows," Nature **406**, 385 (2000).

Mueth, D.M., H.M. Jaeger and S.R. Nagel, "Force distribution in a granular medium," Phys. Rev. E **57** (3), 3164 (1998).

Nott, P. R., and J.F. Brady, "Pressure-driven flow of suspensions: simulation and theory," J. Fluid Mech. **275** 157 (1994).

Nordstrom, K.N., E. Verneuil, P.E. Arratia, A. Basu, Z.Zhang, A.G. Yodh, J.P.Gollub, and D.J. Durian, "Microfluidic rheology of soft colloids above and below jamming," Phys. Rev. Lett. **105** 175701 (2010).

O'Brien, V.T. and M.E. Mackay, "Stress components and shear thickening of concentrated hard sphere suspensions," Langmuir **16**, 7931 (2000).

O'Hern, C.S., S.A. Langer, A.J. Liu, and S.R. Nagel, "Random packings of frictionless particles," Phys. Rev. Lett. **88** (7), 075507 (2002).

O'Hern, C.S., L. E. Silbert, A.J. Liu, and S.R. Nagel, "Jamming at zero temperature and zero applied stress: the epitome of disorder," Phys. Rev. E **68** (1), 011306 (2003).

Onoda, G.Y. and E. G. Liniger, "Random loose packings of uniform sphers and the dilatancy onset," Phys. Rev. Lett. **64** (22), 2727 (1990).

Osuji, C.O., C. Kim, and D. A. Weitz, "Shear thickening and scaling of the elastic modulus in a fractal colloidal system with attractive interactions," Phys. Rev. E **77**, 060402 (2008).

Otsuki, M. and H. Hayakawa, "Critical scaling near jamming transition for frictional particles," arXiv:1006.3597 (2010).

Raghavan, S.R., H.J. Walls, and S.A. Khan, "Rheology of silica dispersions in organic liquids: new evidence for solvation forces dictated by hydrogen bonding," Langmuir **16**, 7920 (2000).

Reynolds, O., "On the dilatancy of media composed of rigid particles," Phil. Mag. **20**, 469 (1885).

Schlichting, H. Boundary Layer Layer Theory. 4th ed., McGraw-hill Book Co., 1960.

Shenoy, S.S. and N.J. Wagner, "Norman J. Wagner Influence of medium viscosity and adsorbed polymer on the reversible shear thickening transition in concentrated colloidal dispersions," Rheol. Acta. **44**, 360 (2005).

Shenoy, S.S., N.J. Wagner, and J.W. Bender, "E-FiRST: Electric field responsive shear thickening fluids," Rheol Acta **42**, 287 (2003).

Singh, A., A. Nir, and R. Semiat, "Free-surface flow of concentrated suspensions," Int. J. Multiphase Flow **32**, 775 (2006).

Smith, M.I., R. Besseling, M.E. Cates, and V. Bertola, "Dilatancy in the flow and fracture of stretched colloidal suspensions,: Nature communications **1**, 114 (2010).

Sperl, M., "Experiments on corn pressure in silo cells – translation and comment of Janssen's paper from 1895," Granular Matter **8**, 59 (2006).

Timberlake, B.D., and J.F. Morris, "Particle migration and free-surface topography in inclined plane flow of a suspension," J. Fluid Mech. **538** 302 (2005).

Trappe, V., V. Prasad, L. Cipelletti, P.N. Segre, and D.A. Weitz, "Jamming phase diagram for attractive particles," Nature **411** 772 (2001).

Van Alsten, J, and S. Granick, "Molecular tribometry of ultrathin liquid films", Phys. Rev. Lett. **61** No. 22, 2570 (1988).

Wagner, N.J. and J.F. Brady, "Shear thickening in colloidal dispersions," Phys. Today, Oct. 2009, 27.

Weitz, D.A., J.P. Stokes, R.C. Ball, and A.P. Kushnick, "Dynamic capillary pressure in porous media: origin of the viscous-fingering length scale," Phys. Rev. Lett. **59** (26), 2967 (1987).

Bischoff White, E.E., M. Chellamuthu, and J.P. Rothstein, "Extensional rheology of a shear-thickening cornstarch and water suspension," Rheol. Acta. **49** 119 (2010).

Zhang, J., T. Majmudar, and R. Behringer, "Force chains in a two-dimensional granular pure shear experiment," Chaos **18**, 041107 (2008).